UiO : Department of Mathematics
University of Oslo

Waves in elastic material

Irregular wavefield propagating from open water into water covered by an elastic sheet

Ingrid Olsen

Master's Thesis, Spring 2019

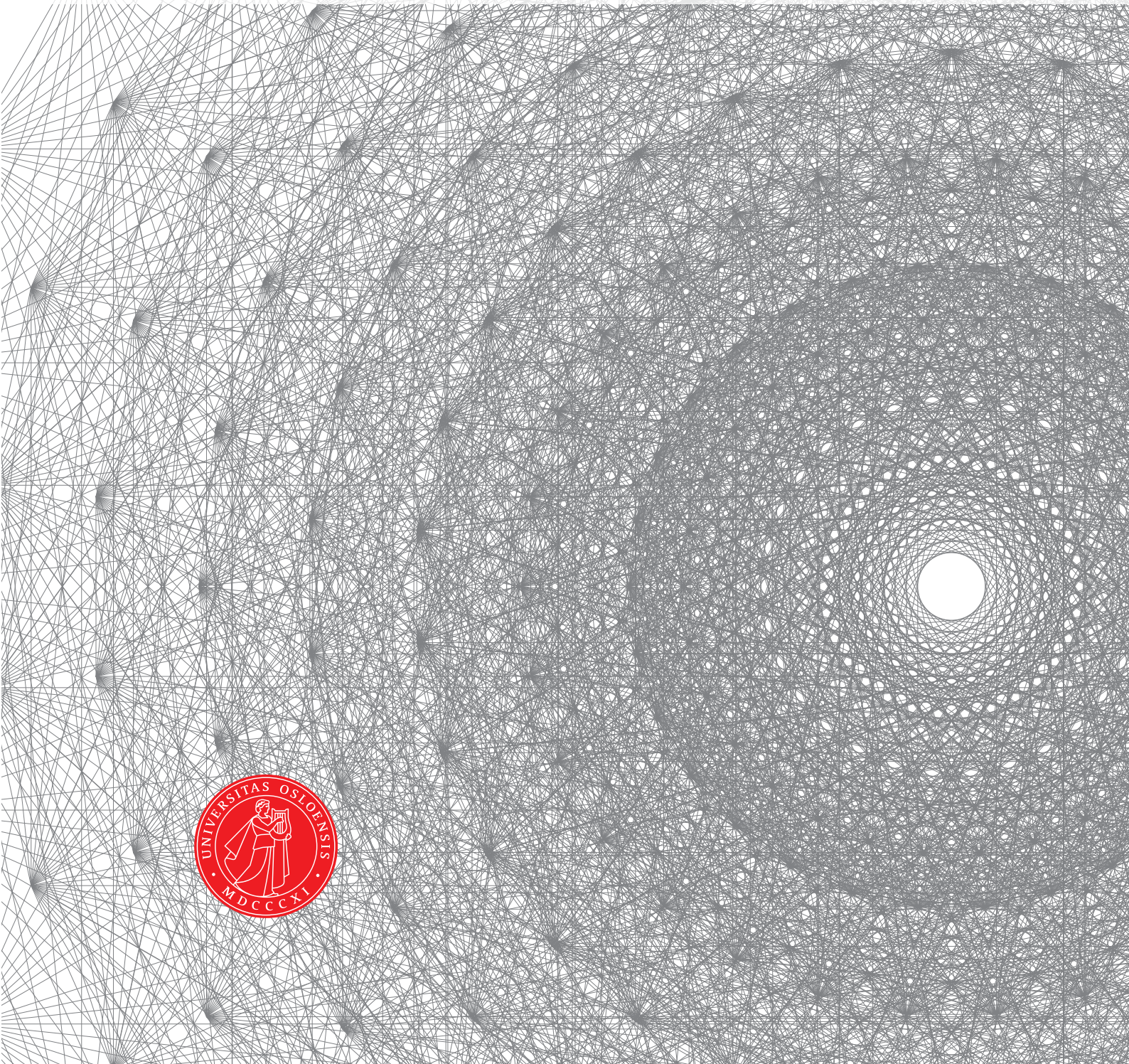

This master's thesis is submitted under the master's programme *Computational Science and Engineering*, with programme option *Mechanics*, at the Department of Mathematics, University of Oslo. The scope of the thesis is 60 credits.

The front page depicts a section of the root system of the exceptional Lie group E_8, projected into the plane. Lie groups were invented by the Norwegian mathematician Sophus Lie (1842–1899) to express symmetries in differential equations and today they play a central role in various parts of mathematics.

Abstract

This thesis presents an experimental investigation on wave-ice interaction and propagation of waves in elastic material. The main purpose of the thesis is to study wave propagation and the energy transition from open water to water covered by an elastic sheet. We also want to unveil if occasions where extreme waves are generated can transpire in elastic material. As waves propagate into ice covered areas they are immidiatly attenuated and energy is lost, we therefore want to find out if energy builds up somewhere inside the elastic cover. For the experiments irregular wavefields based on the JONSWAP-spectrum are used. This provides an approximation to a real sea state as waves are made up by a range of different frequencies, limited by the peak frequency f_p. The surface elevation is then measured and used to investigate statistical properties. In order to compare elastic surface waves with free surface waves, measurements of the same irregular wavefield have also been taken for surface elevation with a free surface.

To understand the movement and propagation of elastic waves in ice the work of *Lui & Mollo Christensen* is used as a starting point, but equations are also derived from the dynamic beam equation. It is concluded that the wave-ice interaction is challenging to describe in full detail, hence some modifications had to be done. Results show that the wavefield gradually adapts to the elastic environment and non-linear effects are found as waves propagates into an elastic cover. It is therefore a possibility for unexpected extreme waves to appear. In addition to deviations in statistical parameters from a Gaussian sea state, instabilities of the wavefield are also found by calculating Benjamin-Feir Index. Attuenuation rates of waves inside the elastic cover are illustrated using frequency and wavenumber-frequency spectrums, in addition to plots of amplitude decay as a function of distance.

Acknowledgements

First of all I would like to thank my supervisor, Professor Karsten Trulsen, for exceptional support, inspiration and guidance. Thank you for introducing me to the fields of extreme waves and wave-ice interaction, and for always being able to help and inspire me during the study and writing of this thesis. I could never have accomplished this without your help and our weekly conversations. In addition I would like to thank Professor Atle Jensen for both introducing me to the field of experimental fluid mechanics and for the research trip to Svalbard. Thank you for giving me the opportunity to experience and study waves in ice in the real life arctic environment. I would also like to thank Olav Gundersen for all the help he has given me in the laboratory, and for making sure we never ran out of coffee!

A huge thanks also goes to my family and friends who have been there for me through my degree. Firstly, I would like to thank my mom Elisabeth, my dad Finn-Rune and my sister Marit for always supporting me and always being there for me. Mom and dad, thank you for the frequent Oslo-visits and phone calls. And Marit, thank you for always making me laugh and turning my mood around even on the worst days! Thank you to all my friends, both from Geology and Mathematics, for five years filled with memories that I will never forget. Luckily there are many more to come!

Ingrid Olsen
Oslo, 15.05.2019

Notation

(x, y, z): Distance in meter
(t): Time in seconds

$\eta(x, t)$: Surface elevation/displacement of surface in form of waves
$\phi(x, z, t)$: Velocity potential of surface elevation
$S(f)/S(\omega)$: One-dimensional spectrum of surface elevation
$S(k, \omega)$: Two-dimensional spectrum of surface elevation
$R(t_1, t_2)/R(\tau)$: Autocorrelation function
$C(t_1, t_2)$: Autocovariance function
$\hat{\eta}(\omega)$: One-dimensional Fourier transform of surface elevation
$\hat{\eta}(k, \omega)$: Two-dimensional Fourier transform of surface elevation

k: Wavenumber
λ: Wavelength
ω: Angular frequency
T: Wave period
f: Frequency
$\tilde{E}$: Mechanical wave energy density
ϵ: Steepness of wave
μ: Expected value
σ: Standard deviation of surface elevation measurements
σ^2/var: Variance of surface elevation measurements
κ: Kurtosis
γ: Skewness
H_s: Significant waveheight
a_c: Characteristic amplitude
τ: Time difference $t_1 - t_2$
δ_ω: Bandwidth
ξ: Angle of curvation
$1/R$: Curvation
$\mathcal{P}$: Stresstensor
$\tilde{\epsilon}$: Strain
g: Gravitational constant
ν: Poissons modulus
E: Youngs modulus/elasticity modulus
β: Kinematic viscosity

Further notation is described in the text where it is applied.

Contents

Chapter 1

Introduction

Waves in the ocean are unpredictable and in some occasions energy can build up and generate unstable wavefields which can be responsible for the formation of large-amplitude water waves, also called extreme or freak waves [27]. It is a fact that these circumstances can occur when waves adapt to new surrondings, for example when propagating from deep to shallow water [22] [11]. Therefore it could be a possibility that these incidents also can transpire when waves propagate into surrondings such as ice, or other types of elastic materials.

1.1 Motivation

Even though we experience ice melting, a big part of the ocean is still covered by ice. Sea ice covers about 7% of the Earth's surface and about 12% of the world's oceans [31]. The understanding of wave propagation in ice is therefore still important to enhance, not only to avoid damage caused by ice breaking but also to understand the impact and evolution of wave movement in elastic material. Investigations of waves propagating into ice covered water have been of increasing interest over the last decade. In addition to an increasing interest in extreme waves, it has become an important topic in engineering and science [16]. The mechanisms and more detailed dynamic properties of extreme waves are clear because of many research efforts [6]. This thesis is an effort to provide more theory and results on wave-ice interaction which can lead to a clearer understanding on how waves adapt to elastic material, and maybe encourage researchers to point further studies in the direction of wave-ice interaction.

1.2 Previous work

Wave-ice interaction and elastic waves in ice are topics of increasing interest, but there is still a lack of research to be found on this subject. It may be the case that the research started in 1986, when a scientist on the *R/V Polarstern* encountered a series of waves with approximately one meter amplitude 560 km away from the ice edge in the Weddell sea. These waves resulted in breakup of the icepack which had a maximum local thickness of 2 meters, and an averaged thickness of 80 cm. The Weddell sea extreme waves have been explained and analysed by *Lui & Mollo-*

Christensen in their article *Wave Propagation in a Solid Ice Pack* [15]. In this article they derive the dispersion relation for waves under pack compression and compare group velocity to critical mean compressive stress, in addition to carrying out a stability analysis using the non-linear cubic Schrödinger equation and providing a non-linear model to describe waves in ice.

Lui & Mollo Christensen's theory has further been used in other articles to provide theory on wave-ice interaction. The MET.no report written by *Broström & Christensen* for Statoil Hydro in 2008 investigates methods and calculations for different types of ice (slush ice, pancake ice etc.) following the equations of *Lui & Mollo Christensen* [15] and *Wadhams et.al.* [32] [4]. A recent paper which does not follow the equations mentioned above, but rather the model of *Wang & Shen* [33], shows an experimental study on gravity waves in a floating viscoelastic cover [23]. This paper provides and discusses wave characteristics, wave celerity and wave attenuation inside a viscoelastic cover. This thesis will later use the results and discussions from this article for comparison.

Wave attenuation has also been an important topic when investigating waves in elastic media. Several studies show an attempt in finding an amplitude-decay function to fit the exponential energy decay of a wavefield inside elastic material, or ice cover. This is done in terms of attenuation in time in *Lui & Mollo-Christensen's* article from 1988 [15], but in this thesis we will be more interested in knowing the spatial attenuation rate. Following *Sutherland et.al.* [25] the spatial attenuation rate of wave amplitude for laboratory experiments with finite dimensions can be written:

$$a(x) = a_0 e^{-\alpha x}, \tag{1.1}$$

where a_0 is the initial amplitude, $\alpha = \beta\sqrt{\frac{\omega}{2\beta}}(\frac{1}{sinh2kH} + \frac{1}{kB})k/c_g$, β is the kinematic viscosity of water, ω is the angular frequency, k is the wavenumber, B is the width of the wave tank and c_g is the group velocity. This attenuation rate is believed to be due to boundary layer dissipation, and will later be used for comparison to the experimental results.

1.3 Research questions

As earlier mentioned, there is still a lack of wave-ice interaction theory. Hopefully this thesis can contribute to the questions regarding the energy transition from open water waves to elastic waves in ice, and propagation of elastic waves in general. In this thesis the wave-ice interaction is investigated experimentally using the big wave tank in the Hydrodynamic laboratory at the University of Oslo. An irregular wavefield is provided from a JONSWAP-spectrum as defined in equation 2.38, with three different peak frequencies. By measuring the surface elevation it is possible to carry out a statistical analysis and compare the results with theoretical values. In order to compare statistical results for elastic waves we measure the same irregular wavefield on a free surface. This provides characteristic values for the wavefield as free surface gravity waves. To approximate ice covered water four different elastic sheets are placed in the tank, hence three different PEHD (polyethylene high density) sheets

and one Latex sheet both with different thicknesses. For each cover all three wavefields with a duration of 15 minutes are measured at several locations (21 locations for PEHD cover and 17 locations for Latex cover). By taking measurements at different locations we are able to investigate the development of elastic waves in space, and hence the development of energy inside the elastic cover can be studied. It is believed that this amount of data will provide a high enough resolution in both the spatial and temporal domain.

1.4 Outline

Chapter 2 presents a short summary of useful mathematical and theoretical concepts applied in this thesis. This include stochastic description of surface waves, an introduction to both stochastic variables and processes, a short introduction to the Fourier transform and descriptions of bandwith and the Benjamin-Feir Index among more.

Chapter 3 contains theory on both free surface waves and the dynamic equation on waves in elastic material. Derivation of the beam equation is included, in addition to calculation of dispersion relation, phase speed and group velocity. The reflection coefficient is also calculated theoretically in this chapter.

In Chapter 4 the arrangements done in order to be able to perform the experiments to provide surface displacement data are explained and accounted for. This includes the setup of experiments, methods for imitating ice cover and for data sampling.

Chapter 5 contains the results from experiments done for this thesis. First experimental conditions are explained, then results are shown. The results are divided into subsections containing characteristic wave parameters, time series of surface elevation and reflection coefficient calculations. Phase speed and group velocity are plotted, in addition to amplitude attenuation. Values for skewness and kurtosis are contained, and plots of power spectral density, wavenumber-frequency spectrum and BFI.

In Chapter 6 discussions on results are presented. First wave characteristics are discussed, in addition to the reflection coefficients. Next topic of discussion is values of skewness and kurtosis, then phase speed and group velocity. The amplitude attenuation is also discussed and lastly non-linear effects are investigated.

The final conclusion of the theisis is contained in Chapter 7, in addition to comments on further work to be done on this subject.

Chapter 2

Mathematical background

From observations of the ocean we know that waves or wavefields are not deterministic, but rather random and unpredictable. We can therefore look at the surface displacement η as a stochastic process with several different outcomes, or realizations, for any selection of times [29]. This chapter provides statistical theory, and a description of surface waves with stochastic parameters used to characterize the wavefield in this thesis.

2.1 Stochastic description of surface elevation

As mentioned the ocean sea surface is random and unpredictable, but even so the model of *random linear wave theory* assumes it to be made up by a superposition of linear, *monochromatic* waves [12]. It should be mentioned that a monochromatic wave is a wave propagating with one frequency only. A superposition of different monochromatic waves then results in a wavefield with a range of frequencies. In this theory we consider the sea surface as a finite sum of plane waves:

$$\eta(x,t) = \sum_{n=1}^{N} a_n cos(k_n x - \omega_n t + \theta_n), \tag{2.1}$$

where a_n represents the amplitudes, θ_n represents the phases, ω_n and k_n represents the angular frequencies and wavenumbers, respectively. The latter two are related through the dispersion relation. The definition (2.1) of surface waves is the first step towards using stochastic theory to describe waves. The phases θ_n are assumed to be independent, stochastic variables uniformly distributed on $[0, 2\pi]$. The amplitudes a_n in eq. (2.1) can be defined in terms of the wave frequency spectrum, or power spectrum [17]:

$$\frac{1}{2}a_n^2 = S(\omega)d\omega = 2\pi S(f)df = \frac{\tilde{E}}{\rho g}. \tag{2.2}$$

In addition to being defined in terms of the wave frequency spectrum, the amplitudes of a wavefield are also defined in terms of the energy $\tilde{E}$. Therefore when studying amplitude development of a wavefield one can also correlate it to development of energy. The wave frequency spectrum is an important concept in this thesis, in addition to the energy development. A more detailed description is hence given in Section 2.4.

2.2 Stochastic variables

First we consider the surface elevation, $\eta(t)$, as the real-valued stochastic process with unpredictable stochastic outcomes for any selection of times t. We can then choose to study only one of the outcomes, for example the stochastic variable $\eta_i = X$ of the stochastic process $\eta(t)$, as the outcome at time $t = t_i$.

The *cumulative distribution function* of the stochastic variable is defined by *Logan* as [14]:

$$F(X) \equiv P\{X \leq x\}, \tag{2.3}$$

where X is the outcome from the stochastic process, and P, the *probability function*, indicates the probability of X being less than or equal to a value x. The derivative of the cumulative distribution function (2.3) is called the *probability density function*, and is again defined by *Logan* [14]:

$$f = \frac{dF}{dx} \tag{2.4}$$

with properties:

$$f(x) \geq 0, \quad \int_{-\infty}^{\infty} f(x)dx = 1. \tag{2.5}$$

The *expected value*, also called the *first moment*, for a stochastic variable is defined as the weighted average:

$$\mu = E[X] = \int_{-\infty}^{\infty} xf(x)dx. \tag{2.6}$$

[29]. A stochastic variable's *variance* is hence defined by:

$$\sigma^2 = Var[X] = E[(X-\mu)^2] = \int_{-\infty}^{\infty} (x-\mu)^2 f(x)dx = E[X] - \mu^2, \tag{2.7}$$

where we assume linearity of the expected value operator E. The standard deviation of the variable is defined as the square root of the variance: $\sigma = \sqrt{\sigma^2}$.

Generally the *n'th moment* of the stochastic variable X is given as:

$$m_n = E[X^n] = \int_{-\infty}^{\infty} x^n f(x)dx, \tag{2.8}$$

while the *n'th central moment* is:

$$\mu_n = E[(X-\mu)^n] = \int_{-\infty}^{\infty} (x-\mu)^n f(x)dx, \tag{2.9}$$

where we also observe that the variance is thus defineable as the second central moment (2.9) of the stochastic variable. Higher moments can also be found from the stochastic variables. *Skewness* is defined as the third central moment (2.9), and

is a measure of the asymmetry of the probability distribution around the real-valued mean of the variable:

$$\gamma = \frac{E[(X-\mu)^3]}{\sigma^3} = \frac{\mu^3}{\sigma^3}. \tag{2.10}$$

Kurtosis is defined as the fourth central moment:

$$\kappa = \frac{E[(X-\mu)^4]}{\sigma^4} = \frac{\mu^4}{\sigma^4}. \tag{2.11}$$

We define excess kurtosis as the kurtosis minus 3. For zero excess kurtosis ($\kappa = 3$) the distribution is said to be mesokurtic. We will also define zero excess kurtosis to be a Gaussian, or normal distribution [20] and the kurtosis of other distributions are often are compared to this value. When $\kappa > 3$ the tails of the propability distribution are more weighted and extreme waves are more likely to develop. Both skewness and kurtosis will be helpful when investigating occurences of extreme wave events through the elastic covers in laboratory experiments.

2.2.1 Stochastic wave parameters

The stochastic parameters of a variable can further be used to calculate important wave characteristics such as *significant wave height* H_s and *characteristic amplitude* a_c. Significant wave height is defined as:

$$H_s = 4\sigma, \tag{2.12}$$

where σ is given from equation (2.7) and characteristic amplitude is calculated as:

$$a_c = \frac{H_s}{2\sqrt{2}}. \tag{2.13}$$

Both significant wave height and characteristic amplitude can provide a measure on how waves are attenuated inside the elastic sheet we want to study wave propagation in. Hence they are used as a measure on energy loss as a function of distance.

2.3 Stochastic process

The surface elevation $\eta(t)$ is now considered as the real-valued stochastic process with several different outcomes for any selection of times t. The outcomes are a collection of stochastic variables, also called an *ensemble* [17]. The process $\eta(t) = X(t)$ is time dependent, where $X(t)$ represents the given ensemble of outcomes for given times t.

The expected value of the real stochastic process $X(t)$ is:

$$\mu(t) = E[X(t)] = \int_{-\infty}^{\infty} x(t) f(x;t) dx. \tag{2.14}$$

The *autocorrelation function* for a real process $\eta(t)$ is given by:

$$R(t_1,t_2) = E[X(t_1)X(t_2)] = \int_{-\infty}^{\infty}\int_{-\infty}^{\infty} x_1 x_2 f(x_1,x_2;t_1,t_2) dx_1 dx_2, \tag{2.15}$$

where X_1 and X_2 are the outcomes for times $t = t_1$ and $t = t_2$. The *mean power* of the process is defined as the second moment:

$$R(t,t) = E[|\ X(t)^2\ |]. \tag{2.16}$$

The *autocovariance function* for a real process is defined as:

$$C(t_1,t_2) = E[(X(t_1) - \mu(t_1))(X(t_2) - \mu(t_2))] \tag{2.17}$$
$$= R(t_1,t_2) + \mu(t_1)\mu(t_2). \tag{2.18}$$

A process is said to be *weakly stationary* if the expected value (2.14) and autocovariance (2.17) does not vary with respect to time. The autocorrelation function is then only dependent on a time difference $\tau = t_1 - t_2$, and not time t explicitly [17]. Similarly, distributions of higher order only depends on time intervals and not on absolute time. We then have:

$$\mu(t) = E[X(t)] = \mu \tag{2.19}$$
$$R(t_1,t_2) = R(\tau). \tag{2.20}$$

For a weakly stationary process the mean power of the process is given by $R(0)$, where $R(0)$ is real and non-negative. We recognize it as the variance of the process in the case where $\mu = 0$. In this thesis we will assume, but not justify, that the surface elevation can be considered as a weakly stationary and *ergodic process*. An ergodic process is defined by an ensemble that can be determined from a single time history [18]. This means that time and ensemble averaging data gives the same result.

2.4 Power spectrum and Fourier transform

The *power spectrum* [17] of a weakly stationary process is defined as the Fourier transform of the autocorrelation function $R(\tau)$. The transform pairs are defined by:

$$S(\omega) = \frac{1}{2\pi}\int_{-\infty}^{\infty} R(\tau)e^{i\omega\tau}d\tau \tag{2.21}$$
$$R(\tau) = \int_{-\infty}^{\infty} S(\omega)e^{-i\omega\tau}d\omega, \tag{2.22}$$

with normalization criterion $R(0) = \int_{-\infty}^{\infty} S(\omega)d\omega$ satisfied. Take notice of the normalization in the first equation (2.21), which is different depending on preference within different research groups. It does not matter which convention one uses as long as one is consistent with the choice. It is also important to mention that different programming languages use different conventions as well. In this thesis we will follow the convention defined above.

A real process has an even spectrum and therefore we can introduce a *one-sided spectrum* for non-negative frequencies. The desired Fourier transform pairs is then:

$$S_{one-sided}(\omega) = \frac{1}{\pi}\int_{-\infty}^{\infty} R(\tau)e^{i\omega\tau}d\tau = \frac{2}{\pi}\int_{0}^{\infty} R(\tau)cos\omega\tau d\tau \tag{2.23}$$
$$R(\tau) = \int_{0}^{\infty} S_{one-sided}(\omega)cos\omega\tau d\omega, \tag{2.24}$$

with the normalization criterion still statisfied, $\int_0^\infty S_{one-sided}(\omega)d\omega = R(0)$.

2.4.1 One-dimensional Fourier transform

The measurements of the surface elevation from the experiments this thesis is based on present surface elevation as a function of time and space. The one-dimensional Fourier transform can thus be used to convert the measured data from the time domain to the frequency or angular frequency domain. The one-dimensional Fourier transform of the function $\eta(t)$ is defined as [17]:

$$\hat{\eta}(\omega) = \int_{-\infty}^{\infty} \eta(t) e^{-i\omega t} dt, \tag{2.25}$$

with its inverse Fourier transform as mentioned earlier:

$$\eta(t) = \frac{1}{2\pi} \int_{-\infty}^{\infty} \eta(\omega) e^{i\omega t} d\omega. \tag{2.26}$$

The Fourier transform can be regarded as an inner product:

$$\hat{\eta}(\omega) = \langle \eta(t), e^{i\omega t} \rangle = \int_{-\infty}^{\infty} \eta(t) e^{-i\omega t} dt. \tag{2.27}$$

Fourier transforms can also be expressed over a finite time interval $[0, \Delta t]$ instead of over an infinite interval. The Fourier transform then becomes:

$$\hat{\eta}(\omega_n) = \langle \eta(t), e^{i\omega_n t} \rangle = \int_0^{\Delta t} \eta(t) e^{-i\omega_n t} dt, \tag{2.28}$$

with its inverse Fourier transform given as:

$$\eta(t) = \frac{1}{\Delta t} \sum_{n=-\infty}^{\infty} \hat{\eta}(\omega_n) e^{i\omega_n t}, \tag{2.29}$$

where $n = 0, 1, 2, \ldots$ is the number of different frequencies f_n contained in the wavefield. The one-dimensional Fourier transform provides the frequency- or angular frequency spectrum ($\omega_n = 2\pi f_n$), and shows how the energy of the wavefield is distributed in the frequency domain.

2.4.2 Two-dimensional Fourier transform

For the two-dimensional Fourier transform the equations are defined the same way, but the transform is then used to convert from both the time- and space domain to the angular frequency- and wavenumber domain.

The two-dimensional Fourier transform can be defined by:

$$\hat{\eta}(k_m, \omega_n) = \int_0^{\Delta t} \int_0^{\Delta x} \eta(x, t) e^{-i\omega_n t} e^{-ik_m x} dx dt, \tag{2.30}$$

with its inverse two-dimensional Fourier transform then given as:

$$\eta(x, t) = \frac{1}{\Delta t} \frac{1}{\Delta x} \sum_{n=-\infty}^{\infty} \sum_{m=-\infty}^{\infty} \hat{\eta}(k_m, \omega_n) e^{i\omega_n t} e^{ik_m x}, \tag{2.31}$$

where $n = 0, 1, 2, \ldots$, and $m = 0, 1, 2, \ldots$ are the numbers of different frequencies f_n and wavenumbers k_m contained in the wavefield, respectively. The two-dimensional Fourier transform $\hat{\eta}(k_m, \omega_n)$ represents the wavenumber-frequency spectrum of the wavefield, which means that it shows the distribution of energy in both the wavenumber and frequency domain.

2.4.3 Bandwidth and BFI

The *bandwidth* of a spectrum $S(\omega)$ is the ratio between the width, $\Delta\omega$, and the centerpoint, ω_p, of the spectrum. This ratio is useful to know when analysing the power spectrum and instability of the surface elevation. The bandwidth is a dimensionless parameter defined by:

$$\delta_\omega = \frac{\Delta\omega}{\omega_p}. \tag{2.32}$$

A good method to find $\Delta\omega$ is the "half-height-half-width" method [19]. This method measures the width of the spectrum at half of the maximum height of the frequency spectrum, and defines this width as twice the bandwidth. A spectrum is said to be narrowbanded if the bandwidth $\delta_\omega \ll 1$ [29], which means that the spectral density is concentrated to a small frequency band around the peak frequency f_p. If the bandwidth $\delta_\omega \gg 1$ the specrum is hence broadbanded, which means that the spectrum consists of more widespread frequencies than for a narrowband spectrum.

Bandwidth δ_ω is further used to calculate the *Benjamin-Feir Index* (henceforth BFI) of the wavefield. As the surface elevation measurements used in this thesis are measurements of a homogen and stationary irregular wavefield, the wavefield can be subject to modulation instability [3]. Modulation or sideband instability is a phenomenon where deviations from a periodic waveform are reinforced by nonlinearities. This eventually leads to generation of spectral-sidebands and eventual breakup of the wavefield which can result in the generation of extreme waves [5]. BFI is used as an indicator for instability of the wavefield and is defined as the ratio between *steepness*, ϵ, and bandwidth of the measured surface elevation [1]:

$$BFI = \frac{\epsilon}{\delta_\omega}. \tag{2.33}$$

2.5 The central limit theorem

It is demanded that the surface elevation is a sum of independent and identically distributed random variables with mean μ and variance σ^2. The central limit theorem then states that the limiting distribution of the surface elevation η is defined as the normal, Gaussian distribution [14]. A *Gaussian distribution* with mean μ and variance σ^2 has a probability density function given by:

$$f(x) = \frac{1}{\sqrt{2\pi}\sigma} e^{-\frac{(x-\mu)^2}{2\sigma^2}}. \tag{2.34}$$

The ocean is often described by a Gaussian distribution, or referred to as a Gaussian sea state. This sea state refers to a normal distributed stochastic process with

skewness γ equal to zero and kurtosis κ equal to three [18]. Therefore we often mention excess kurtosis when discussing the fourth moment. Excess kurtosis is the kurtosis minus 3, and for zero excess we have $\kappa = 3$, as in a Gaussian state (2.11) as earlier mentioned.

The central limit theorem and the Gaussian sea state are important for the results of this thesis as it defines the ocean sea surface as being normal distributed. Any deviations from Gaussian statistics will imply that the central limit theorem (2.34) breaks down and the assumptions are no longer valid. Deviation from Gaussian statistics is what we are seeking to find for wave propagation on the surface covered by an elastic sheet.

2.6 Spectral models

For a fully developed sea the spectrum of a wavefield is a function of dimensionless frequency only. The *Pierson-Miskowitz spectrum* assumes a fully developed sea, while the *JONSWAP-spectrum* assumes that the sea is still in a developing state [18]. For the remainder of this section, we will comment on these two spectrums which are of great importance when generating the wavefield applied in this thesis.

2.6.1 Pierson-Moskowitz spectrum

The Pierson-Moskowitz spectrum is a unimodal spectrum with a formulation developed from analysis of weather ship data in the North Atlantic [18]. It is defined as:

$$S_{PM}(f) = \frac{\alpha}{f_p^5} exp[-\frac{\beta}{f_p^4}], \tag{2.35}$$

where α and β are constants related to the main sea parameters. The constants are usually set to be:

$$\alpha = \frac{5}{16} H_s^2 f_p^4 \tag{2.36}$$

$$\beta = \frac{5 f_p^4}{4}, \tag{2.37}$$

where f_p is the peak frequency and H_s is the significant wave height defined as $H_s = 4\sqrt{\sigma^2}$, where σ^2 is the zeroth moment of the frequency spectrum or the variance (2.7). It is further assumed that this spectrum is narrowbanded with Rayleigh distributed wave heights.

2.6.2 JONSWAP spectrum

The JONSWAP spectral formulation is based on a wave measurement program known as the Joint North Sea Wave Project [9]. It was carried out in 1968-1969 and represents a developing sea state with fetch limitations, where wind speed and fetch length are inputs to the formulation [18]. The fetch length is the length of the

water over which a given wind has blown. This spectrum is defined as:

$$S(f) = \frac{\alpha}{f_p^5} exp[-\frac{\beta}{f_p^4}]\gamma^{-(f-f_p)^2/2\sigma^2 f_p^2} \tag{2.38}$$

$$\sigma = 0.07, \ \omega \leq \omega_p \tag{2.39}$$

$$\sigma = 0.09, \ \omega > \omega_p, \tag{2.40}$$

which may be recognized as the Pierson-Moskowitz spectrum (2.35) multiplied with $\gamma^{-(f-f_p)^2/2\sigma^2 f_p^2}$, called the peak enchancement factor. The peak enhancement factor γ is usually set to $\gamma = 3.3$, hence also used in this thesis. This is the spectrum used to simulate the data file of surface elevation used in the experiments. The JONSWAP-spectrum plotted from the experimental input-file is shown in Figure 2.1 below.

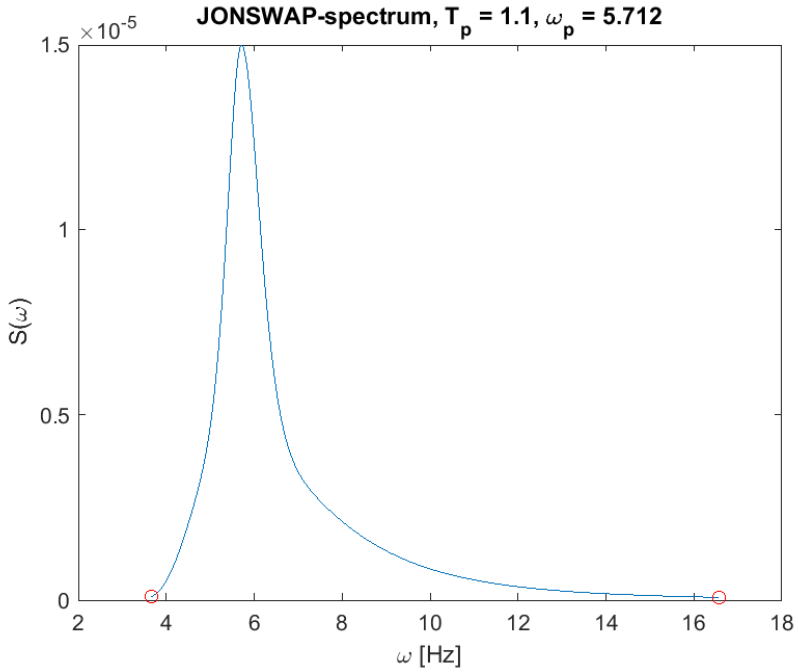

Figure 2.1: JONSWAP-spectrum calculated from data file applied in experiments to provide surface elevation.

Chapter 3

Wave theory

In this chapter analytical calculations are explained to provide an understanding about the problem of waves propagating from a free surface into an ice cover, or in this case an elastic cover. General theory on surface gravity waves are included, in addition to theory on waves propagating into covered water. To understand the motion of the sheets imitating ice cover, equations are derived from the dynamic beam equation [10] and compared to the equations by *Lui & Mollo-Christensen* [15].

3.1 A 3D problem

The boundary value problem of waves propagating from a free surface into a covered surface can be visualized as a three dimensional problem. We assume uniformity in y-direction so that waves only propagate in x-direction and the surface elevation is given by $\eta(x,t)$. A figure of the problem with all spatial directions is shown in Figure 3.1, where the wave generator is on the far left (symbolized by the red star), and on the far right there is an absorbing beach reducing wave reflection from the end of the tank. The elastic sheet is placed approximately in the middle of the tank and is illustrated by the black area covering eight meters of the water surface.

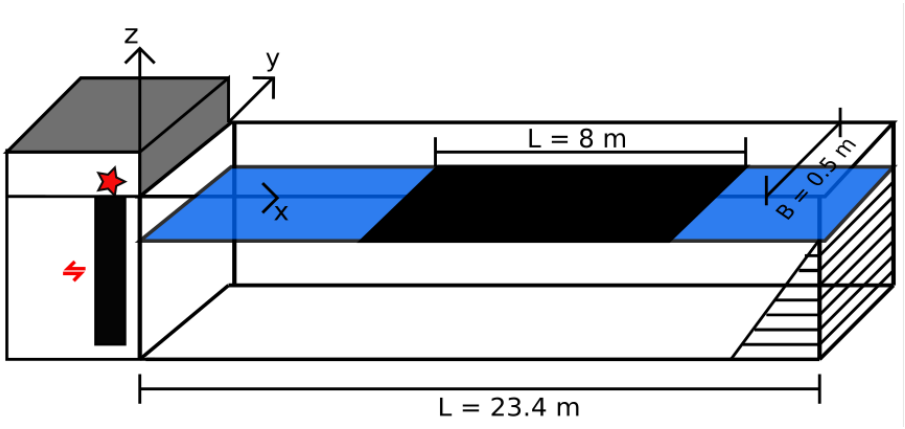

Figure 3.1: Illustration of wave tank with coordinate system.

3.2 Free surface gravity waves

The following section provides general information on wave characteristics, explains both the variables used in analytical methods and the derivation of boundary conditions for gravity waves on a free surface.

3.2.1 Surface wave characteristics

The *wave equation* is given by:

$$\frac{\partial^2 \eta}{\partial t^2} - c^2 \nabla^2 \eta = 0, \tag{3.1}$$

and can describe wave propagation in a medium with constant propagation speed c. There are several solutions of this equation and therefore several ways to describe waves. Following random linear wave theory we assume a solution made up by a superpositon of *Stokes waves* on deep water. Stokes waves are often given as:

$$\eta(x,t) = a\big(cos\theta + \frac{1}{2}(ka^2)cos2\theta + \mathcal{O}(ka^3)\big), \tag{3.2}$$

where a denotes amplitude and $\theta = kx - \omega t$ is the phase function, where k is the wavenumber and ω is the angular frequency. Wavenumber k and angular frequency ω are associated with wavelength and waveperiod as $k = \frac{2\pi}{\lambda}$ and $\omega = \frac{2\pi}{T}$ [28].

In this thesis we will be interested in knowing wave characteristics such as characteristic amplitude a_c and characteristic wavenumber k_c to find wave steepness $\epsilon = k_c a_c$. This quantity provides information on the degree of non-linearities in the wavefield [21].

3.2.2 Dispersion relation

The *characteristic wavenumber* is set equal to k_p, which is the peak wavenumber. Peak wavenumber is the wavenumber that corresponds to the maximum angular frequency, ω_p and is found by using the *linear dispersion relation* for surface gravity waves:

$$\omega_p^2 = k_p g \ \tanh k_p h. \tag{3.3}$$

The dispersion relation (3.3) must be fulfilled in order for waves to be free. The term linear dispersion relation means that the relation between angular frequency and wavenumber is independent of the wave amplitude. If there is an amplitude dependence the relation is thus non-linear.

For further calculations on the wavefield we need to define the boundary between deep and shallow water. The characteristic dimensionless parameter for wave depth is given by $k_p h$ [21]. Traditionally this parameter decides whether the wavefield is on deep or shallow water. For this thesis the dispersion relation is assumed to be linear and the wavefield is generated on deep water. The dispersion relation could, in a case where $k_p h \gg 1$, be simplified to $\omega_p^2 = k_p g$ since $\tanh k_p h \approx 1$ as $k_p h \to \infty$. Because simplifications are only valid as $k_p h \to \infty$, the dispersion relation is used in its entirety as defined in (3.3).

3.2.3 Conditions

For waves on a free surface the wave motion is constrained by *continuity* and conservation of water mass, hence $\nabla^2\phi = 0$ for $z < \eta$, where ϕ is the velocity potential. The pressure from overlying air can be found by using *Bernoulli's equation* for potential flow given as:

$$\frac{p - p_a}{\rho_a} + \frac{\partial\phi}{\partial t} + \frac{1}{2}v^2 + g\eta = 0. \tag{3.4}$$

Since we know that pressure at the surface equals the atmospheric pressure, $p = p_a$, and in addition to the assumption of small velocities such that $v^2 \ll 1$, the equation that represents the *dynamic boundary condition* becomes:

$$\frac{\partial\phi}{\partial t} + g\eta = 0, \quad z = \eta. \tag{3.5}$$

The *kinematic boundary condition* is found by assuming that all particles at the surface stay there and move with the surface speed. In this case we look at one specific particle at the surface, $z_p = \eta(x_p, t)$, affected by a small displacement Δz_p:

$$z_p + \Delta z_p = \eta(x_p + \Delta x_p, t + \Delta t) = \eta(x_p, t) + \frac{\partial\eta}{\partial x}\Delta x_p + \frac{\partial\eta}{\partial t}\Delta t. \tag{3.6}$$

On the surface, $z_p = \eta$, this reduces to:

$$\Delta z_p = \frac{\partial\eta}{\partial x}\frac{\partial x_p}{\partial t}\Delta t + \frac{\partial\eta}{\partial t}\Delta t, \tag{3.7}$$

which gives us:

$$w = u\frac{\partial\eta}{\partial x} + \frac{\partial\eta}{\partial t}, \quad z = \eta, \tag{3.8}$$

where $u = \frac{\partial x_p}{\partial t}$ and $w = \frac{\partial z_p}{\partial t}$. If we now assume that the wavelengths are small compared to water depth, we know that the term $u\frac{\partial\eta}{\partial x}$ is much smaller than $\frac{\partial\eta}{\partial t}$ and further $u\frac{\partial\eta}{\partial x} \ll w$. Therefore the kinematic boundary condition becomes:

$$\frac{\partial\phi}{\partial z} = \frac{\partial\eta}{\partial t}, \quad z = \eta. \tag{3.9}$$

If we perform a Taylor-expansion of ϕ around $z = 0$, where we can neglect higher order terms, it can be shown that both the dynamic and kinematic boundary condition, eq. (3.5), (3.9), are also applicable at $z = 0$. For illustration the expansion is carried out for the dynamic boundary condition:

$$\frac{\partial\phi}{\partial t}\,|_{z=\eta} = \frac{\partial\phi}{\partial t}\,|_{z=0} + \eta\frac{\partial^2\phi}{\partial t\partial z}\,|_{z=0} + \frac{\eta^2}{2}\frac{\partial^3\phi}{\partial t\partial z^2}\,|_{z=0}\,. \tag{3.10}$$

3.3 Elastic waves

Waves propagating into water covered by an elastic sheet can not be analysed using the regular wave equation with the free surface conditions. There are additional terms in the equation of motion for the elastic sheet and several conditions that must be taken into consideration. In this section the boundary value problem for waves on a covered elastic surface is explained in detail motivated by the dynamic beam equation [10] and the equations of *Lui & Mollo-Christensen* [15].

3.3.1 Conditions

To be able to derive equations for the sheet-covered surface it must be assumed that the *Navier-Bernoullis hypothesis* is valid and that the sheet is linear elastic, which means application of Hooke's law. We must also assume small displacements in the sheet, hence a small surface elevation.

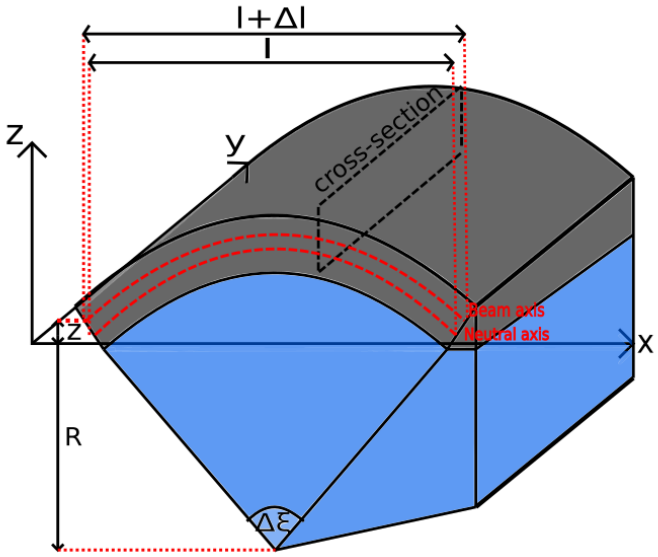

Figure 3.2: Illustration of an element from the 3D covered water problem.

The ends of the sheet are assumed to be attached, hence there are no torques on the sheet from the end points. As mentioned earlier we assume uniformity in y-direction, and the water under the sheet will provide pressure from underneath. Air lying above the sheet is assumed to not provide any forces. Since water is incompressible, the movement of the sheet will be constrained by conservation of water mass and hence $\nabla^2\phi = 0$. To summarize all conditions four hypothesises are made [10]:

1. *Deformation hypothesis I*
   Navier-Bernoulli's hypothesis must be assumed fulfilled, as described in Section 3.3.2.

2. *Deformation hypothesis II*
   Gradient of curvation z is much less than 1, which means that the incline ξ is small enough to use the approximation: $\tan\xi = \xi = \frac{\partial z}{dx} \ll 1$.

3. *Stress hypothesis*
   Normal stress on surfaces parallel with the beam axis can be neglected.

4. *Material hypothesis*
   The material is linear elastic, which means Hooke's law can be applied.

3.3.2 Navier-Bernoulli's hypothesis

Following *Irgens* [10] we derive the *beam equation* by assuming small deformations, to further be able to define curvation and stress in a beam, or in this case an elastic sheet, affected by deformation. Assuming small deformations the equations can be simplified. Navier-Bernoulli's or Bernoulli's hypothesis involves the consequences of making this assumption, and must be fulfilled for *Deformation hypothesis I* (1) to be valid. The curvation, or deformation, to study in the elastic sheet is $z = \eta(x, y, t) = \eta(x, t)$ because of uniformity of wave motion in the y-direction. The dynamic beam equation is derived using the plane of wave propagation, the xz-plane, where the cross-section constant, I, is defined in the uniform yz-plane.

From figure 3.2 we define the *neutral surface* to be the surface in the yz-plane with no deformation in the deformated xz-plane, $\Delta l = 0$. The *beam axis* is defined to be the deformation axis where the material parallel with this axis changes length from l to $l + \Delta l$. The neutral surface cuts a cross-section in the neutral axis and goes through the *cross-section area centre*. Along the neutral axis the stress equals zero [10].

If we study the bending of a beam with curvation centre underneath the beam (as shown in figure 3.2) the *bending radius* of a curve $z = \eta(x, t)$ is given as:

$$\frac{1}{R} = -\frac{\frac{d^2z}{dx^2}}{[1 + (\frac{dz}{dx})^2]^{3/2}}. \tag{3.11}$$

If we now assume small deformations (2), $(\frac{dz}{dx})^2 \ll 1$, the bending radius can be simplified to:

$$\frac{1}{R} = -\frac{d^2z}{dx^2}. \tag{3.12}$$

A direct consequence of this assumption is that a cross-section surface which is plane and normal to the neutral axis before bending will maintain its characteristics after deformation. The length of the beam axis before deformation is $l = \Delta\xi R$, with corresponding angular deformation:

$$\Delta\xi = \frac{l}{R}. \tag{3.13}$$

After deformation the extension is given by $\Delta l = \Delta\xi(R+z) - \Delta\xi R$, and the angular deformation becomes:

$$\Delta\xi = \frac{l + \Delta l}{R + z}. \tag{3.14}$$

The strain in x-direction is consequently:

$$\tilde{\epsilon} = \frac{\Delta l}{l} = \frac{\Delta\xi(R + z) - \Delta\xi R}{\Delta\xi R} = \frac{z}{R}. \tag{3.15}$$

For cross-section surfaces plane and normal to the neutral axis there are no change in length, $\Delta l = 0$, therefore the strain is:

$$\tilde{\epsilon} = 0. \tag{3.16}$$

If we now use the assumption of a linear elastic sheet (4), Hooke's law can be used to define corresponding stress [7]. We can then write:

$$\mathcal{P} = E\tilde{\epsilon} = E\frac{z}{R}, \tag{3.17}$$

where E is the *elasticity module*. Hence is the stress of the beam in x-direction a linear function of the curvature $z = \eta(x,t)$, and hence is a plane cross-section surface also plane and normal to the neutral axis after bending caused by small deformations, because these surfaces are not affected by any stress.

For a thin sheet, rather than a beam, the thickness of the sheet, h_i, and deformation η are small compared to the length of the sheet. If the sheet is streched in x-direction, the streching will be compensated by compression in y-direction. We then have:

$$\tilde{\epsilon}_x = \frac{1}{E}(\mathcal{P}_x + \nu\mathcal{P}_y), \tag{3.18}$$

where stress in y-direction is defined by *Poisson's module* ν times the negative stress from streching in x-direction, $\mathcal{P}_y = -\nu\mathcal{P}_x$. Therefore the non-thin direction, x-direction, is said to resists the Poisson effect. Inserting for $\mathcal{P}_y$ and $\tilde{\epsilon}_x$ from (3.15) leads to the stress:

$$\mathcal{P}_x = \frac{E}{(1-\nu^2)}\tilde{\epsilon}_x = \frac{E}{(1-\nu^2)}\frac{z}{R}. \tag{3.19}$$

3.3.3 External force from water pressure

The pressure from water under the sheet can be described using Bernoulli's equation (3.4) for non-stationary potential flow:

$$\frac{p_w}{\rho_w} + g\eta + \frac{1}{2}\boldsymbol{v}^2 = C, \tag{3.20}$$

where C is a constant, the flow is irrotational $\nabla \times \boldsymbol{v} = 0$ hence $\boldsymbol{v} = \nabla\phi$. ϕ represents the velocity potential of the flow in the water as an effect from the wave motion η. Including evolution in time:

$$\frac{\partial\phi}{\partial t} + \frac{p_w}{\rho_w} + g\eta + \frac{1}{2}\boldsymbol{v}^2 = C. \tag{3.21}$$

Inserting the velocity potential where $\frac{1}{2}\boldsymbol{v}^2 = \frac{1}{2}(\nabla\phi)^2$ and Taylor-expanding the time-derivative around equilibrium, $z = 0$:

$$\frac{\partial\phi}{\partial t}\,|_{z=\eta} = \frac{\partial\phi}{\partial t}\,|_{z=0} + \eta\frac{\partial^2\phi}{\partial t\partial z}\,|_{z=0} + \frac{\eta^2}{2}\frac{\partial^3\phi}{\partial t\partial z^2}\,|_{z=0}, \tag{3.22}$$

where we have assumed η only provides small displacements. We can therefore write:

$$\frac{\partial\phi}{\partial t}\,|_{z=\eta} = \frac{\partial\phi}{\partial t}\,|_{z=0}\,. \tag{3.23}$$

Assuming small displacements we can also neglect non-linear terms in the equation, as we then also assume small velocities, $\frac{1}{2}(\nabla\phi)^2 \ll 1$. We then get:

$$\frac{\partial\phi}{\partial t} + \frac{p_w}{\rho_w} + g\eta = C = 0 \tag{3.24}$$

$$p_w = -\rho_w(\frac{\partial\phi}{\partial t} + g\eta),, \tag{3.25}$$

which is the equation (3.25) for the external force imposed from underlying water pressure.

3.3.4 Dynamics of elastic waves

Because of the sheets elasticity and rigidity we have three more forces that must be implemented to the equation of motion. First we consider neglected normal forces as mentioned in the *Stress hypothesis* (3):

$$\int_A \mathcal{P}_{xx}dA = \int_A \mathcal{P}_{zz}dA = N = 0, \tag{3.26}$$

which gives the *stress-tensor* for the beam or elastic sheet:

$$\mathcal{P} = \begin{bmatrix} \mathcal{P}_{xx} & \mathcal{P}_{xz} \\ \mathcal{P}_{zx} & \mathcal{P}_{zz} \end{bmatrix} = \begin{bmatrix} 0 & \mathcal{P}_{xz} \\ \mathcal{P}_{zx} & 0 \end{bmatrix} \tag{3.27}$$

The *bending moment* must also be considered, and can be derived using the result of Navier-Bernoulli's hypothesis. Remember that we assume $h_i \ll l$ and $z \ll l$, l being length in x-direction, so that the stress of bending (3.19) is given by:

$$\mathcal{P}_{xz} = \frac{E}{(1-\nu^2)}\tilde{\epsilon}_{xz} = \frac{E}{(1-\nu^2)}\frac{z}{R} \tag{3.28}$$

$$\int_A (\mathcal{P}_{xz}\cdot z)dA = \int_A E\frac{z^2}{(1-\nu^2)R}dA = \frac{E}{(1-\nu^2)R}\int_A z^2dA = M, \tag{3.29}$$

where M denotes the *bending moment*. The shear stress is always equal such that $\mathcal{P}_{xz} = \mathcal{P}_{zx}$. The equations will be derived for only one of the shear directions but applies to both.

Lastly we have the *cross-section constant*, also called the second moment of area:

$$I = I_z = \int_A z^2dA. \tag{3.30}$$

With parameters from experiments done for this thesis we get the cross-section constant defined as:

$$I = \int_0^b \int_{-\frac{h}{h}}^{\frac{h}{2}} z^2dzdy = \frac{b}{3}z^3\,|_{z=-\frac{h}{2}}^{z=\frac{h}{2}} = \frac{b}{3}(\frac{h}{2})^3 2 = \frac{bh^3}{12}, \tag{3.31}$$

where h is the thickness of the beam, or in this case the elastic sheet, and b is the beam or sheets width. We continue to refer the cross-section constant, or the second

moment of area as I (3.31).

Further we can write the bending moment (3.29) as: $\frac{EI}{(1-\nu^2)R} = M$, which is the *bending moment equation* and further gives the bending radius $\frac{1}{R} = \frac{M(1-\nu^2)}{EI}$ [10]. The sheets bending or flexibility is consequently proportional to the bending moment (3.29) and reverse proportional to the sheets flexural rigidity. From the stress in x-direction we know that $E = \frac{\mathcal{P}_{xz}(1-\nu^2)R}{z}$, inserting this into the bending moment gives the *stress of bending formula*:

$$\mathcal{P}_{xz} = \frac{M}{I}z. \tag{3.32}$$

We define the sheets bending or curvation to be $\frac{1}{R} = \frac{M(1-\nu^2)}{EI}$ and assume that the incline of the sheet decreases in positive x-direction, $d\phi = -\frac{ds}{R}$, where ds is the element length. The differential therefore gives negative curvature:

$$\frac{d\phi}{ds} = -\frac{1}{R} = -\frac{M(1-\nu^2)}{EI}. \tag{3.33}$$

Deformation hypothesis II (2) implies $ds = dx$: $\frac{d\phi}{dx} = \frac{\partial^2 z}{\partial x^2}$, and hence we obtain the *differential equation for the elastic line* which regards surfaces parallel with the beam axis:

$$\frac{\partial^2 z}{\partial x^2} = -\frac{M(1-\nu^2)}{EI}. \tag{3.34}$$

Generally the bending moment is a function of x, $M = M(x)$ and can be defined by a set of differential equations with a partitioned external load $f^v = q(x,t)$ [10]:

$$\frac{\partial V}{\partial x} = -q(x,t), \tag{3.35}$$

where V is the *shear force* on the sheet.

$$\frac{\partial M}{\partial x} = V(x) \rightarrow \frac{\partial^2 M}{\partial x^2} = -q(x,t). \tag{3.36}$$

From the differential equation for the elastic line (3.34) we get:

$$\frac{EI}{(1-\nu^2)}\frac{\partial^2 z}{\partial x^2} = -M \tag{3.37}$$

$$\frac{\partial^2}{\partial x^2}\Big(\frac{EI}{(1-\nu^2)}\frac{\partial^2 z}{\partial x^2}\Big) = -\frac{\partial^2 M}{\partial x^2} = q(x,t). \tag{3.38}$$

Then inserting for $z = \eta(x,t)$ and adding the acceleration term for the elastic sheet, where $\mu = h_i\rho_i$, the *modified dynamic beam equation* is defined as:

$$\mu\frac{\partial^2 \eta}{\partial t^2} + \frac{\partial^2}{\partial x^2}\Big(\frac{EI}{(1-\nu^2)}\frac{\partial^2 \eta}{\partial x^2}\Big) = q(x,t). \tag{3.39}$$

In this thesis the external load $q(x,t)$ is neglected as the air does not provide any force on the sheet. And finally, adding the pressure (3.25) from the underlying

water, the equation of motion for the elastic sheet becomes:

$$\mu\frac{\partial^2\eta}{\partial t^2} + \frac{EI}{(1-\nu^2)}\frac{\partial^4\eta}{\partial x^4} = p_w \tag{3.40}$$

$$\mu\frac{\partial^2\eta}{\partial t^2} + \frac{EI}{(1-\nu^2)}\frac{\partial^4\eta}{\partial x^4} = -\rho_w(\frac{\partial\phi}{\partial t} + g\eta). \tag{3.41}$$

Because the strain arising from streching, $\nu\mathcal{P}_{yy}$, can be assumed much smaller than the strain from wave propagation, $\mathcal{P}_{xz}$, one can neglect the compression in y-direction for experiments with finite dimensions. This is where the equations differ from the equations used by *Lui & Mollo-Christensen* [15]. We then have:

$$\mu\frac{\partial^2\eta}{\partial t^2} + EI\frac{\partial^4\eta}{\partial x^4} = -\rho_w(\frac{\partial\phi}{\partial t} + g\eta). \tag{3.42}$$

The equation of motion (3.42) is also known as the dynamic boundary condition for the elastic waves at $z = 0$. In addition to this condition, the kinematic boundary condition (3.9) from the free surface waves also holds:

$$\frac{\partial\phi}{\partial z} = \frac{\partial\eta}{\partial t}, \ z = \eta, \ z = 0 \tag{3.43}$$

and as earlier mentioned water mass is conserved such that $\nabla^2\phi = 0$ for $z < \eta$, where η now is at the bottom of the elastic sheet.

3.3.5 Dispersion relation

Assuming a monochromatic wave solution as:

$$\eta(x,t) = a\sin(kx - \omega t), \tag{3.44}$$

with velocity potential on the form:

$$\phi(x,z,t) = -be^{kz}\cos(kx - \omega t), \tag{3.45}$$

where we also assume that the kinematic boundary condition (3.9) underneath the sheet also holds in time:

$$\frac{\partial}{\partial t}(\frac{\partial\phi}{\partial z}) = \frac{\partial^2\eta}{\partial t^2} \rightarrow -bk\omega = -a\omega^2. \tag{3.46}$$

Implementing this into the equation of motion for the elastic sheet (3.42) gives us:

$$\mu\frac{\partial^2\eta}{\partial t^2} = -\omega^2\mu a\sin(kx - \omega t), \tag{3.47}$$

$$EI\frac{\partial^4\eta}{\partial x^4} = EIk^4 a\sin(kx - \omega t), \tag{3.48}$$

$$-\rho_v(\frac{\partial\phi}{\partial t} + g\eta) = -\rho_v(-b\omega e^{kz}\sin(kx - \omega t) + ga\sin(kx - \omega t)). \tag{3.49}$$

Multiplication with k for all terms, and taking in account that the lower sheet lies at $z = 0$ results in:

$$-\rho_v k(\frac{\partial\phi}{\partial t} + g\eta) = -\rho_v(-b\omega k\sin(kx - \omega t) + gka\sin(kx - \omega t). \tag{3.50}$$

We can then use the kinematic boundary condition (3.9) at $z = 0$ which gives:

$$-\rho_v k(\frac{\partial \phi}{\partial t} + g\eta) = -\rho_v(-a\omega^2 \sin(kx - \omega t) + gka \sin(kx - \omega t). \tag{3.51}$$

After some rearranging we end up with the dispersion relation for waves in the elastic sheet:

$$-\omega^2 \mu k + EIk^5 = -\rho_v(-\omega^2 + gk) \tag{3.52}$$

$$\omega^2 = \frac{gk\rho_v + EIk^5}{\rho_v + \mu k}. \tag{3.53}$$

It should be mentioned that it is not certain if these equations are enough to describe waves in elastic material. This topic is much discussed and equations as the non-linear Schrödinger and modified non-linear Schrödinger are also frequently used [15] [2] [13]. Hopefully, when presenting the results and comparing with theoretical values it will show which equations are in agreement with waves in elastic material.

3.3.6 Phase speed and group velocity

As for the free surface waves both *phase speed* and *group velocity* of the waves can be calculated from the dispersion relation. From theory [21] we know that:

$$c_p = \frac{\omega}{k}, \tag{3.54}$$

is the phase velocity, and the group velocity is the dispersion relation derivated with respect to the wavenumber k:

$$c_g = \frac{d\omega}{dk}. \tag{3.55}$$

Inserting the dispersion relation in each of these equations, (3.54) and (3.55), provides two equations for phase speed and group velocity respectively:

$$c_p = \frac{(gk\rho_v + EIk^5)^{\frac{1}{2}}}{(\rho_v + \mu k)^{\frac{1}{2}}} \cdot \frac{1}{k}. \tag{3.56}$$

Derivating the dispersion relation with respect to k using partial derivation:

$$c_g = \omega'(k) = \frac{u'(k)v(k) - u(k)v'(k)}{\big(v(k)\big)^2}, \tag{3.57}$$

where $u(k) = gk\rho_v + EIk^5$ and $v(k) = rho_v + \rho_i h_i k$.
Derivating u and v and inserting into the equation gives:

$$c_g = \big[\frac{g\rho_v + 5EIk^4}{2\sqrt{gk\rho_v + EIk^5}} \cdot \sqrt{\rho_v + \rho_i h_i k} - \frac{\sqrt{gk\rho_v + EIk^5} \cdot \rho_i h_i}{2\sqrt{\rho_v + \rho_i h_i k}}\big] \cdot \frac{1}{\rho_v + \rho_i h_i k}. \tag{3.58}$$

3.4 Reflection at boundary

To be able to calculate the amount of energy reflected at the boundary between open water and water covered by an elastic sheet we calculate the *reflection coefficient*, assumed to be the ratio [19]:

$$\frac{R}{I} \tag{3.59}$$

where I is the incoming complex amplitude, and R is the reflected complex amplitude. Since the reflected amplitudes are assumed to be smaller than the amplitudes of the incoming waves, the reflection coefficient should be a number between 0 and 1. In order to find this ratio the Fourier transform of the measured surface elevation is used.

3.4.1 Theoretical reflection coefficient

Assuming the incoming wavefield defined as the surface elevation:

$$\eta(x,t) = Ie^{i(kx-\omega t)} + Re^{i(-kx-\omega t)}. \tag{3.60}$$

Where I and R are the amplitudes of the incoming and reflected waves respectively. Taking the inverse Fourier transform accomplishes independence of angular frequency of the surface elevation function:

$$\hat{\eta} = <\eta(x,t), e^{-i\omega t}> = \frac{1}{\Delta t}\int_0^{\Delta t} \eta(x,t)e^{i\omega t}dt \tag{3.61}$$

$$= \frac{1}{\Delta t}\int_0^{\Delta t} \left(Ie^{i(kx-\omega t)} + Re^{i(-kx-\omega t)}\right)e^{i\omega t}dt \tag{3.62}$$

$$\hat{\eta} = \frac{1}{\Delta t}(Ie^{ikx} + Re^{-ikx}), \tag{3.63}$$

where wavenumber k and angular frequency ω are related by the dispersion relation (3.3). Measuring surface elevation $\eta(x,t)$ at two different locations, that is $x = 0$ and $x = d$ gives us:

$$\eta(0,t) = \eta_0 = \frac{1}{\Delta t}(Ie^{i(-\omega t)} + Re^{i(-\omega t)}) \tag{3.64}$$

$$\eta(d,t) = \eta_d = \frac{1}{\Delta t}(Ie^{i(kd-\omega t)} + Re^{i(-kd-\omega t)}), \tag{3.65}$$

with corresponding Fourier transforms:

$$\hat{\eta_0} = \frac{1}{\Delta t}(I + R) \tag{3.66}$$

$$\hat{\eta_d} = \frac{1}{\Delta t}(Ie^{ikd} + Re^{-ikd}). \tag{3.67}$$

Eliminating R or I in these two equations, which means multiplying $\hat{\eta_0}$ with $e^{\pm ikd}$, provides equations for the complex amplitudes R and I:

$$R = \frac{\hat{\eta_d} - \hat{\eta_0}e^{ikd}}{e^{-ikd} - e^{ikd}} \tag{3.68}$$

$$I = \frac{\hat{\eta_0}e^{-ikd} - \hat{\eta_d}}{e^{-ikd} - e^{ikd}}, \tag{3.69}$$

and finding the reflection coefficient to be:

$$\frac{R}{I} = \frac{\hat{\eta_d} - \hat{\eta_0} e^{ikd}}{\hat{\eta_0} e^{-ikd} - \hat{\eta_d}}. \tag{3.70}$$

Note that $\hat{\eta_0}$ and $\hat{\eta_d}$ are the Fourier coefficients representing the highest energy in the Fourier transform (frequency domain) of two surface elevations measured at $x = 0$ and $x = d$, respectively. In addition the amplitudes R and I becomes complex amplitudes when performing a Fourier transform.

3.4.2 Singular points

As we derive the reflection coefficient, $\frac{R}{I}$, we notice that the complex amplitudes have singularities in the denominator of the fraction for both R and I. If this equals zero we have singular points in our calculations. The denominator can be written as:

$$e^{-ik\Delta x} - e^{ik\Delta x} = -2i \sin(k\Delta x). \tag{3.71}$$

Having this expression equal to zero gives the singular points:

$$-2i \sin(k\Delta x) = 0 \rightarrow k\Delta x = \pi n, \tag{3.72}$$

which means that there are singularities in the reflection coefficient for each $\Delta x = \frac{\pi n}{k}$ where $n = 1, 2, \ldots, N$ and Δx is the distance between measurements. When these singular distances are discovered it is possible to avoid them by placing the probes at different locations, which do not provide singular values in calculations of the reflection coefficient.

Chapter 4

Experimental arrangements

This chapter provides information and descriptions of the experimental work done, in order to provide surface displacement data to this thesis. All experiments are carried out in the Hydrodynamic Laboratory at the University of Oslo, where wave propagation is generated with a WaveLab system. In addition to experimental arrangements, this chapter also includes explanations on how the surface displacement data is post processed.

4.1 Experimental setup

For the investigation of wave propagation in elastic material the big wave tank in the Hydrodynamic Laboratory at the University of Oslo is used. The wave tank is 23.4 meters long and 0.5 meters wide. The water depth can be adjusted and is chosen to be $h = 0.7$ meters in these particular experiments to provide deep water waves. An illustration of the wave tank is shown in figure 4.1 below.

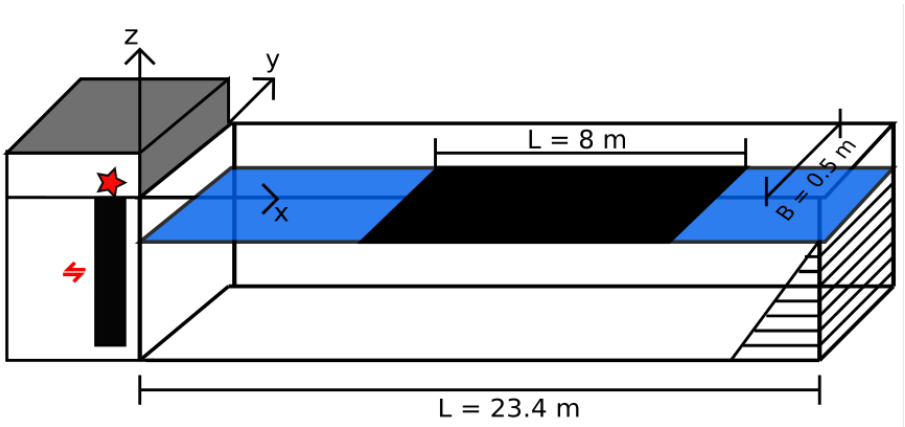

Figure 4.1: Illustration of wave tank with all spatial directions

At the end of the tank, at the far right in figure 4.1, there is an absorbing beach reflecting 3% of the incoming waves [8]. On the left side of the tank the hydraulic wave generator is installed. This generator induces a field of surface waves into the tank and is controlled by WaveLab software, where manual input of frequency and amplitude generates regular waves. An irregular wavefield, which is applied in this thesis, can also be generated by supplying WaveLab with numerically generated

input signals. Explanation of input signals and numerical code are to be found in Appendix A.

The x-axis is chosen to be the longitudinal direction of the wave tank with the z-axis pointing upwards as the vertical axis. We define $z = 0$ at the mean water level. We assume uniformity in y-direction and therefore analyse the experiment in two dimensions, in the xz-plane, as shown in figure 5.1.

4.2 Methods

4.2.1 Elastic covers

To approximate ice covered water PEHD (polyethylen high density) 300 sheets are placed into the tank. Three different sheets of this type are used with different thicknesses, being 1, 2 and 3 mm. In addition to the PEHD sheets, a thin Latex sheet is also used with thickness 0.2 mm. Important properties of the two types of elastic sheets are shown in Table 4.1 below:

Property of sheet	PEHD	Latex
Thickness $[mm]$	1,2,3	0.2
Density $[kg/m^3]$	940	960
E-module $[N/m^3]$	0.8	0.0015
Possion's ratio	0.45	0.5

Table 4.1: Properties of elastic sheets used in experiments.

4.2.2 Surface elevation measurements

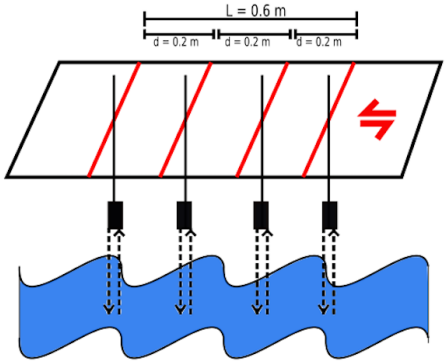

Figure 4.2: Moveable skeleton consisting of four probes over water surface.

To measure the surface elevation a setup consisting of 4 USS02/HFP, IP 65, M18 x 1.0 wave ULS Advanced probes, also called gauges, delivered by Ultralab were used, with a techincal resolution of 0.18 mm. The scan rate of the probes can be chosen to either 125 Hz or 250 Hz, whith a measuring range between 30 mm and 250 mm. We will in this experiment use a sampling rate of 125 Hz. The wave probes send

out an ultrasonic pulse and measures the time, t, it takes to recieve the transmitted signal. The transport time, t, is then used to calculate the distance from the surface by comparing it to the mean level. The four wave probes are placed as shown in Figure 4.2 with a distance of 0.2 meters between them. The probes are attached to a movable skeleton which is placed at different locations making a overlapping grid towards the beach to get high resolution results. For the PEHD sheet a three-probe overlapping grid is used as shown in Figure 4.3, and for the Latex sheet a two-probe overlapping grid is used as shown in Figure 4.4. This grid arrangement is used because of attachments in the PEHD sheets which we do not want to include in the measurements.

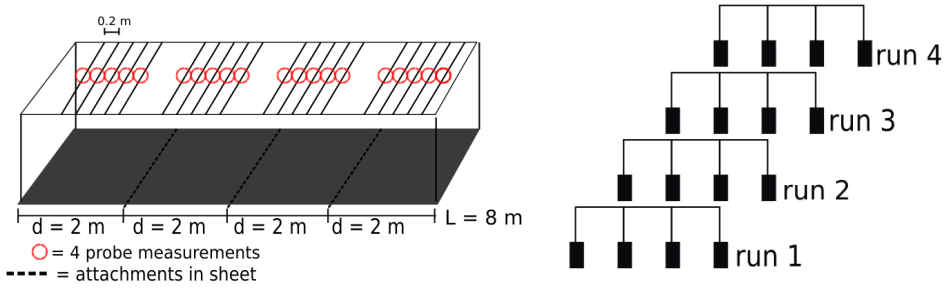

Figure 4.3: Measurement locations and measurement grid for PEHD sheets, in total 20 locations on the sheet.

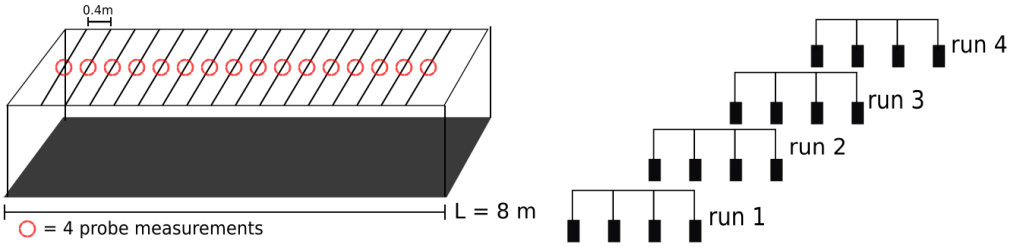

Figure 4.4: Measurement locations and measurement grid for Latex sheet, in total 16 locations on the sheet.

An advantage using this particular system when measuring surface elevation is the possibility to connect multiple probes to the same channel. If the transmitted signal from the surface is reflected outside of the transmitting wave probe range, one of the other probes connected to the same channel might recieve it. This means that the amount of dropouts can be reduced if the geometry of the waves causes reflections outside the range of the transmitting probe. Four probes connected to four different channels are used in experiments for this thesis, mainly because the waves applied are far from breaking. Hence geometry of the waves does not cause reflections outside the transmitting probe range.

It is believed that the surface elevation generated in the tank is the most unstable close to the wave generator and at the very beginning of propagation, which is why the start of measurements are triggered 30 seconds after generating the first

waves and measurments are taken eight meters away from the generator. This reduces startup effects and assures that the wavefield is stable when measuring surface elevation.

4.3 Post processing of data

When post processing the data measured by the probes MatLab is used. The files are imported as *csv*-files, and for each location a 885 seconds long time series of surface elevation is provided. With a sampling rate of 125 Hz the resolution in the time domain is $\Delta t = 0.008$ and gives 110612 values for surface elevation in time. In the spatial domain the resolution is constrained by number of locations in the wave tank. For all sheets we have 4 probes per location with a spatial distance of 0.2 meters and an overlapping grid. For PEHD sheets the resolution is $\Delta x = 4.8$ which gives 96 values in x-direction and for the Latex sheet the resolution is $\Delta x = 7.2$ which gives 115 values.

To reduce noise and dropouts from the data the function "InterpolateDropouts" is used (see Appendix B for details). Calculations are done and inbuilt functions in MatLab are used to find statistical parameters for surface elevation, attenuation of energy inside the elastic sheet and to visualize the results.

4.4 Sources to error

In both the experiments and in the post processing of data done for this thesis there are some sources to error to be taken into consideration. First of all the interpolation of dropouts that occur in the measurements can result in giving a false picture of the surface elevation. Interpolating dropouts only give an approximation of the true surface elevation that is measured. Luckily, there was a very small amount of dropouts in the data provided for this thesis. Measurements of surface elevation are taken approximately in the middle of the tank, where the width is measured to be 0.5 meters. When generating the wavefield in the wave tank it is assumed that we only have wave propagation in x-direction, which means that waves propagating across the wavetank are not taken into account. For some experimental incidents a small amount of water from the propagating waves splashed over the elastic sheet, making a thin film of water on top of the front sheet. This is not considered in the dynamic equations for elastic sheets. Other sources to error are dissipation of waves and wall friction from the wave tank. In addition we also have friction between the elastic sheet and underlying water. The measured surface elevation for wave propagation in the elastic sheet also shows a great amount of attenuation, this must be taken into consideration when studying the experimental results. None of the sources to error mentioned above are justified in this thesis.

Chapter 5

Experimental results

The experiments for this thesis are designed to investigate wave propagation in an elastic sheet to approximate waves in ice covered water. To approximate the waves in the tank to a real life wavefield, the JONSWAP-spectrum is used [9]. This spectrum provides propagation of an irregular wavefield consisting of a variety of frequencies with a given peak frequency, f_p. Three different peak frequencies are used to simulate the wavefield, hence $f_p = 0.9$ Hz , 1.0 Hz and 1.1 Hz. Measurements of wave propagation in PEHD sheets are done at 21 different locations, one location over open water and 20 locations over the elastic sheet. For the Latex sheet, surface elevation is measured at 17 different locations, one location over open water and 16 locations over the elastic sheet.

In this chapter, the experimental conditions for this thesis will be presented and the results will be obtained. This includes calculated characteristic wave parameters and time series of surface elevation, in addition to calculated reflection coefficient at the boundary between open water and water covered by the elastic sheet. Wave phase speed and group velocity plots are provided, in addition to plots of spatial amplitude attenuation rates. Values for statistical parameters such as skewness and kurtosis are also calculated and presented in this chapter. Power spectral density, in addition to wavenumber-frequency spectrum are plotted for different locations in the wave tank. Lastly the stability of the wavefield is investigated by calculating the Benjamin-Feir Index (BFI).

5.1 Experimental conditions

The input files, based on the JONSWAP-spectrum [9], are made in MatLab with constant parameters. Only peak period, or peak frequency, is changed. Table 5.1 shows an overview of the parameters that are used to simulate the JONSWAP-spectrum. All experiments are carried out using the big wave tank in the Hydrodynamic laboratory at the University of Oslo, as earlier mentioned. For all experiments a water depth of $h = 0.7$ m is used to provide wave systems in the deeper domain, $k_p h > 1$.

In this thesis we would like to investigate how waves propagate into an elastic material and if the wave characteristics change with propagation distance. We therefore use two different types of elastic sheets with different elasticity modulus and with four different thicknesses. For each sheet (see Table 5.2), hence thicknesses

3, 2, 1 and 0.2 mm, wavefields with peak periods $T_p = 1.1$ s, 1.0 s and 0.9 s are used. From here on we refer to the different sheets as $PEHD_1 = 1$ mm, $PEHD_2 = 2$ mm, $PEHD_3 = 3$ mm and $Latex = 0.2$ mm, where the number refers to thicknesses for the PEHD sheets.

Parameter for JONSWAP-spectrum	Value
Time duration, T [s]	885
Intensity of spectrum, α	0.001
Peak enhancement factor, γ	3.3
Shape factor, β	1.25

Table 5.1: Parameters used in all JONSWAP-files to provide surface elevation in the wave tank.

Sheet type	Thickness [mm]	T_p [s]	T_p [s]	T_p [s]
PEHD	3	1.1	1.0	0.9
PEHD	2	1.1	1.0	0.9
PEHD	1	1.1	1.0	0.9
Latex	0.2	1.1	1.0	0.9

Table 5.2: Sheet types with thicknesses and peak periods used to provide surface elevation for the experiments.

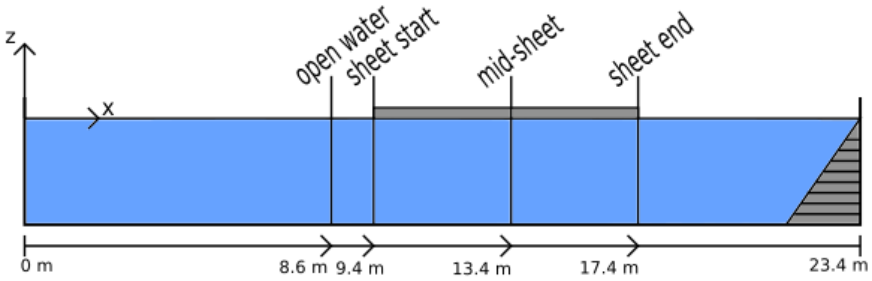

Figure 5.1: Illustation of the wave tank with locations and distances in meters for calculations done for both sheets. Wave paddle is installed on the left side (at 0 meters) and a damping beach to reduce reflection is located at the right side of the wave tank.

5.1.1 Calculations

To be able to analyse the wave system and its characteristics different wave parameters such as peak frequency f_p, peak wavenumber k_p and significant waveheight H_s are calculated. All calculation methods and calculated parameters are presented in Table 5.3. The power spectrum is calculated using Welch's method, where peak frequency f_p is found. Welch's method and the power spectrum are explained in more detail in Subsection 5.2.7.

Parameter	Calculation
Peak frequency f_p $[s^{-1}]$	Maximum value from spectrum
Peak angular frequency ω_p $[s^{-1}]$	$\omega_p = 2\pi f_p$
Peak wavenumber k_p $[m^{-1}]$	From dispersion relation
Peak wavelength λ_p $[m]$	$\lambda_p = \frac{2\pi}{k_p}$
Significant waveheight H_s $[mm]$	$H_s = 4\sigma$
Characteristic amplitude a_c $[mm]$	$a_c = \frac{H_s}{2\sqrt{2}}$
Steepness ϵ	$\epsilon = a_c k_p$
Benjamin-Feir Index (BFI)	$BFI = \frac{\epsilon}{\delta_\omega}$

Table 5.3: Wave parameters provided for specified locations on each sheet and for each period.

5.1.2 Amplitude attenuation

To compare characteristic amplitude caluclations to theoretical values the attenuation curve of *Sutherland et.al.* is used (1.1) [25], where the kinematic viscosity is used as a free variable. Table 5.4 shows values for kinematic viscosity, β, used to produce the best fit of the attenuation rate curve to the measurements.

Sheet type	$T_p = 1.1$s	$T_p = 1.0$s	$T_p = 0.9$ s
Latex	$5 \cdot 10^{-4}$	$3 \cdot 10^{-3}$	$3 \cdot 10^{-3}$
$PEHD_1$	$5 \cdot 10^{-3}$	$9 \cdot 10^{-3}$	$1 \cdot 10^{-2}$
$PEHD_2$	$5 \cdot 10^{-3}$	$5 \cdot 10^{-3}$	$5 \cdot 10^{-3}$
$PEHD_3$	$6 \cdot 10^{-3}$	$5 \cdot 10^{-3}$	$4 \cdot 10^{-3}$

Table 5.4: Values for kinematic viscosity, β $[m^2 s^{-1}]$, for each experimental incident used to fit the attenuation curve to measurements.

5.2 Results

The results obtained from experiments will now be presented. Because of a big amount of results, the section is divided into subsections to provide overview and structure. Each subsection will be presented properly and contains results for the given subsection only. It should be mentioned that all results are compared to reference measurements. Reference measurements are of the same irregular wavefield used for elastic sheets, but propagating on a free surface. In the plots, these reference measurements are located before a black dashed line, representing the start of the elastic sheets at $x = 1$.

5.2.1 Characteristic wave parameters

Since it is necessary to investigate the characteristic properties of the wavefield as a function of distance, wave parameters are calculated from measurements on open water, at the start of the elastic sheet, at the middle of the sheet and at the end of the sheet (distances shown in Figure 5.1). The locations on the elastic sheets with distances are shown in Figures 4.3 and 4.4. The measurements are done at several different locations to be able to characterize the wavefield of elastic waves and to investigate the effect of attenuation inside the sheet.

5.2.1.1 Free surface reference measurements

To be able to analyse characteristic wave parameters for waves propagating into an elastic sheet we have to compare the data with some threshold values. Therefore measurements of the same irregular wavefield are taken with a free surface, and with no elastic sheet in the tank. Wave parameters calculated from measurements of free surface gravity waves, consisting of the same irregular wavefield used in the experiments with elastic sheets, are presented in Table 5.5 below. These parameters are used as threshold values in the comparison with the characteristic parameters for waves in elastic material.

Parameter	$T_p = 1.1$ s	$T_p = 1.0$ s	$T_p = 0.9$ s
$f_p\ [s^{-1}]$	0.916	0.977	1.099
$\omega_p\ [s^{-1}]$	5.752	6.135	6.903
$k_p\ [m^{-1}]$	3.429	3.871	4.867
$\lambda_p\ [m]$	1.832	1.623	1.291
$H_s\ [mm]$	14.336	10.501	7.365
$a_c\ [mm]$	5.069	3.712	2.604
ϵ	0.017	0.014	0.012

Table 5.5: Measurements of gravity waves with free surface used as reference measurements for values calculated with elastic sheet.

5.2.1.2 PEHD$_1$

Parameter	Open water	Sheet start	Mid-sheet	Sheet end
$\mathbf{T_p = 1.1\ s}$				
$f_p\ [s^{-1}]$	0.916	0.870	0.778	0.702
$\omega_p\ [s^{-1}]$	5.752	5.465	4.890	4.410
$k_p\ [m^{-1}]$	3.429	3.055	2.445	1.990
$\lambda_p\ [m]$	1.832	2.063	2.582	3.181
$H_s\ [mm]$	13.326	7.499	4.301	2.563
$a_c\ [mm]$	4.712	2.651	1.520	0.906
ϵ	0.016	0.008	0.003	0.002
$\mathbf{T_p = 1.0\ s}$				
$f_p\ [s^{-1}]$	0.977	0.977	0.855	0.778
$\omega_p\ [s^{-1}]$	6.136	6.136	5.368	4.890
$k_p\ [m^{-1}]$	3.871	3.851	2.954	2.445
$\lambda_p\ [m]$	1.623	1.632	2.150	2.582
$H_s\ [mm]$	10.417	4.560	2.117	1.142
$a_c\ [mm]$	3.683	1.612	0.749	0.404
ϵ	0.014	0.006	0.002	0.001
$\mathbf{T_p = 0.9\ s}$				
$f_p\ [s^{-1}]$	1.083	0.992	0.961	0.641
$\omega_p\ [s^{-1}]$	6.807	6.232	6.040	4.027
$k_p\ [m^{-1}]$	4.738	3.984	3.750	2.210
$\lambda_p\ [m]$	1.329	1.594	1.710	2.844
$H_s\ [mm]$	7.513	2.679	1.302	0.662
$a_c\ [mm]$	2.656	0.947	0.460	0.234
ϵ	0.013	0.004	0.001	0.0005

Table 5.6: Wave parameters for sheet type PEHD$_1$ with all peak periods measured and calculated at four different locations in the wave tank.

5.2.1.3 PEHD$_2$

Parameter	Open water	Sheet start	Mid-sheet	Sheet end
T_p = 1.1 s				
f_p $[s^{-1}]$	0.915	0.885	0.854	0.778
ω_p $[s^{-1}]$	5.752	5.560	5.369	4.889
k_p $[m^{-1}]$	3.429	3.174	2.954	2.458
λ_p $[m]$	1.832	1.989	2.127	2.599
H_s $[mm]$	13.369	4.980	2.990	1.984
a_c $[mm]$	4.7267	1.760	1.057	0.701
ϵ	0.016	0.006	0.003	0.002
T_p = 1.0 s				
f_p $[s^{-1}]$	0.977	0.977	0.946	0.854
ω_p $[s^{-1}]$	6.136	6.136	5.944	5.369
k_p $[m^{-1}]$	3.871	3.866	3.630	2.969
λ_p $[m]$	1.623	1.625	1.738	2.160
H_s $[mm]$	10.630	3.866	1.686	1.214
a_c $[mm]$	3.758	1.079	0.596	0.429
ϵ	0.015	0.004	0.002	0.001
T_p = 0.9 s				
f_p $[s^{-1}]$	1.113	1.037	0	0.244
ω_p $[s^{-1}]$	6.998	6.519	0	1.534
k_p $[m^{-1}]$	5.004	4.376	0	0.966
λ_p $[m]$	1.258	1.446	0	6.504
H_s $[mm]$	6.397	2.035	0.848	0.608
a_c $[mm]$	2.261	0.719	0.299	0.214
ϵ	0.011	0.003	0	0.0002

Table 5.7: Wave parameters for sheet type PEHD$_2$ with all peak periods measured and calculated at four different locations in the wave tank.

From Table 5.6, 5.7 and 5.8 it can be observed that peak frequency f_p decreases as waves propagate into the elastic sheet for all thicknesses, and as a function of spatial distance. Wavenumber k_p also decreases as a function of distance, and the length of the waves increases so the wavefield gradually consists of larger wavelengths as it propagates into the sheet. Significant waveheight H_s is highly decreasing for all three PEHD sheets. It is more decreasing for peak periods $T_p = 1.1$ s than for $T_p = 0.9$ s. Characteristic amplitude a_c decreases aswell, and the most rapid decrease of this parameter is found at the boundary between open water and the start of the sheet. Steepness ϵ is also decreasing as waves propagate into a the elastic media, and is approximately zero at the end of the sheet.

5.2.1.4 PEHD$_3$

Parameter	Open water	Sheet start	Mid-sheet	Sheet end
T_p = 1.1 s				
f_p $[s^{-1}]$	0.915	0.869	0.854	0.625
ω_p $[s^{-1}]$	5.752	5.464	5.368	3.931
k_p $[m^{-1}]$	3.429	3.073	2.120	2.119
λ_p $[m]$	1.832	2.051	2.120	2.965
H_s $[mm]$	13.837	3.592	2.329	1.719
a_c $[mm]$	4.892	1.270	0.823	0.607
ϵ	0.017	0.003	0.002	0.001
T_p = 1.0 s				
f_p $[s^{-1}]$	0.977	0.977	0.946	0.641
ω_p $[s^{-1}]$	6.135	6.135	5.944	4.026
k_p $[m^{-1}]$	3.871	3.880	3.642	2.230
λ_p $[m]$	1.623	1.619	1.732	2.817
H_s $[mm]$	8.672	1.881	1.349	1.140
a_c $[mm]$	3.066	0.665	0.477	0.403
ϵ	0.012	0.002	0.001	0.0009
T_p = 0.9 s				
f_p $[s^{-1}]$	1.083	1.022	1.007	0.717
ω_p $[s^{-1}]$	6.807	6.423	6.327	4.506
k_p $[m^{-1}]$	4.738	4.259	4.133	2.807
λ_p $[m]$	1.329	1.479	1.526	2.238
H_s $[mm]$	6.797	1.327	0.855	0.766
a_c $[mm]$	2.403	0.469	0.302	0.271
ϵ	0.011	0.002	0.001	0.0007

Table 5.8: Wave parameters for sheet type PEHD$_3$ with all peak periods measured and calculated at four different locations in the wave tank.

As mentioned the same characteristics as for PEHD$_1$ can also be observed for PEHD$_2$ and PEHD$_3$. For the decreasing parameters, which are peak frequency f_p, peak wavenumber k_p, significant waveheight H_s, characteristic amplitude a_c and wave steepness ϵ, one can observe that the amount of decrease is greatest for PEHD$_3$, and least for PEHD$_1$. Summed up the decrease of characteristic wave parameters is a function of thickness of the sheets. For PEHD$_2$ the zero peak frequency f_p was dominating the wavefield at the middle of the sheet for $T_p = 0.9$ s. Therefore the values for some of the parameters at this location could not be calculated.

5.2.1.5 Latex

Parameter	Open water	Sheet start	Mid-sheet	Sheet end
$\mathbf{T_p = 1.1\ s}$				
$f_p\ [s^{-1}]$	0.916	0.916	0.915	0.854
$\omega_p\ [s^{-1}]$	5.752	5.752	5.752	5.368
$k_p\ [m^{-1}]$	3.429	3.375	3.375	2.940
$\lambda_p\ [m]$	1.832	1.862	1.862	2.130
$H_s\ [mm]$	13.858	13.042	11.124	8.869
$a_c\ [mm]$	4.899	4.611	3.932	3.136
ϵ	0.017	0.016	0.013	0.009
$\mathbf{T_p = 1.0\ s}$				
$f_p\ [s^{-1}]$	0.977	0.977	0.977	0.977
$\omega_p\ [s^{-1}]$	6.136	6.136	6.136	6.136
$k_p\ [m^{-1}]$	3.871	3.840	3.840	3.840
$\lambda_p\ [m]$	1.623	1.636	1.636	1.636
$H_s\ [mm]$	9.942	9.115	7.382	5.811
$a_c\ [mm]$	3.515	3.223	2.610	2.054
ϵ	0.014	0.012	0.010	0.007
$\mathbf{T_p = 0.9\ s}$				
$f_p\ [s^{-1}]$	1.098	1.098	1.038	1.038
$\omega_p\ [s^{-1}]$	6.902	6.902	6.519	6.519
$k_p\ [m^{-1}]$	4.867	4.861	4.336	4.336
$\lambda_p\ [m]$	1.291	1.292	1.449	1.449
$H_s\ [mm]$	6.881	6.157	4.676	3.460
$a_c\ [mm]$	2.433	2.177	1.653	1.223
ϵ	0.012	0.010	0.007	0.005

Table 5.9: Wave parameters for sheet type Latex with all peak periods measured and calculated at four different locations in the wave tank.

From Table 5.9 one can observe that f_p, k_p, H_s, a_c and ϵ are decreasing parameters, which is the same trend as for the PEHD sheets but the decrease is much less for the Latex sheet. The peak frequency f_p is approximately constant for all peak periods T_p, but is slowly decreasing as a function of distance for $T_p = 1.1$ s and $T_p = 0.9$ s. The wavenumber k_p is also approximately constant through the sheet, but is slowly decreasing, as a function of distance. It can be noticed that the rapid decrease in significant waveheight H_s and characteristic amplitude a_c is not to be found for the Latex sheet, but both are slowly decreasing as a function of distance. Wave steepness ϵ is less decreasing in the Latex sheet than for PEHD sheets, but still a significant decrease is found.

5.2.2 Time series

When studying the time series of surface elevations in the elastic sheets it can be observed a typical attenuation effect, inceasing with thickness of the sheet. For the Latex sheet we have no effect of this becuase the thickness is almost negligable and the sheet more or less follows the surface displacement. For the PEHD sheets the attenuation occurs as a result of sheet stiffness and the natural frequency of the sheet. The stiffness is included in the equations for the sheet by the E-module value.

5.2.2.1 Free surface reference measurements

For all wavefields, wich means JONSWAP-spectrums with peak periods 1.1 s, 1.0 s and 0.9 s, measurements are taken on a free surface in the wave tank with no elastic sheet and at locations in front of the elastic sheet. Data provided for this thesis consists of four probes measuring surface elevations for each location. A time series plot of one location (four probe measurements) and a plot of surface elevation from only one probe is shown in Figure 5.2 and 5.3, respectively.

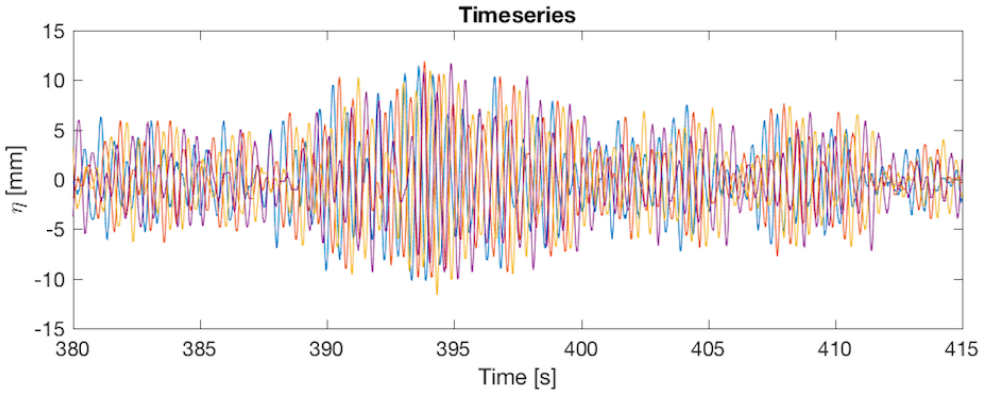

Figure 5.2: Time series plot of all four probes per location. Measurements taken on free surface.

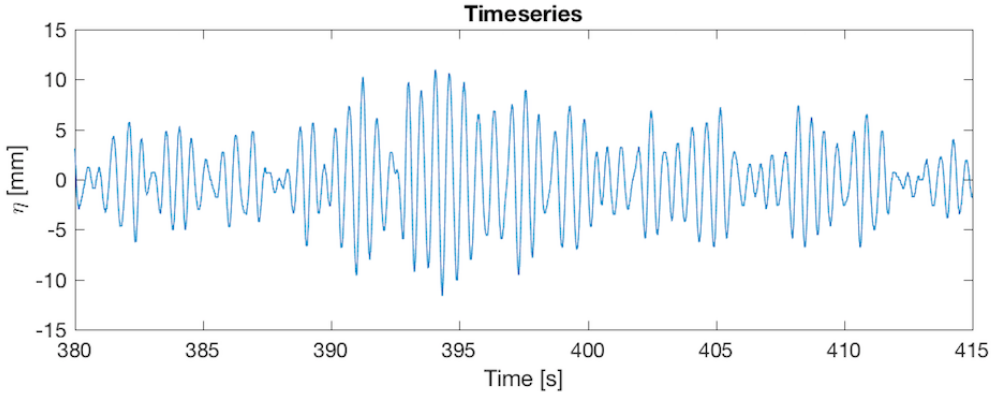

Figure 5.3: Time series plot of one probe. Measurements taken on free surface.

5.2.2.2 PEHD sheets

For all PEHD sheets, with thickness $1, 2$ and 3 mm, the effect from stiffness of the sheet occur at the very beginning of the sheet (location 1). Figure 5.4 shows effects of the wave attenuation as waves propagate into the PEHD sheets with an E-modul equal to 0.8 GPa. These measurements are taken at location 1. Figure 5.5 and 5.6 show surface elevation measurements taken at mid-sheet (location 10) and at the end of the sheet (location 20), respectively. We notice that the amplitudes are "cut off" and that they are replaced by small amplitudes on top of a bigger amplitude. This is an effect of the waves being constrained by the elastic sheet. Waves are attenuated as they propagate into a surface covered by a material with different mechanic and elastic properties. Effect of attenuation also increases with distance, hence for locations close to the sheet end the natural movement of the sheet is even more noticeable, and the waves are almost completely attenuated.

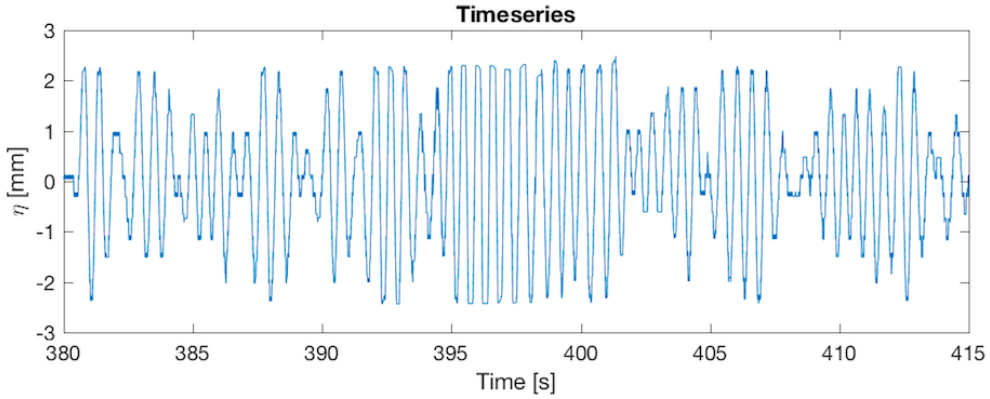

Figure 5.4: Effect of attenuation and stiffness on elastic sheets. Measurements taken at sheet start, location 1

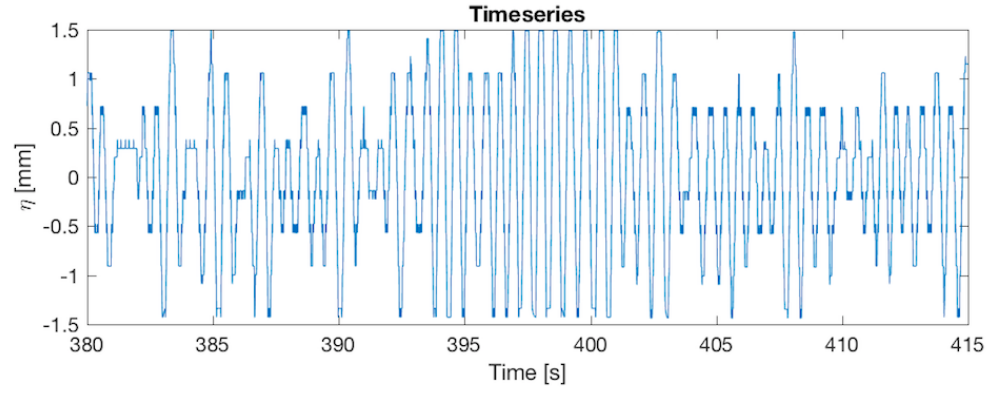

Figure 5.5: Effect of attenuation and stiffness on elastic sheets. Measurements taken at mid-sheet, location 10

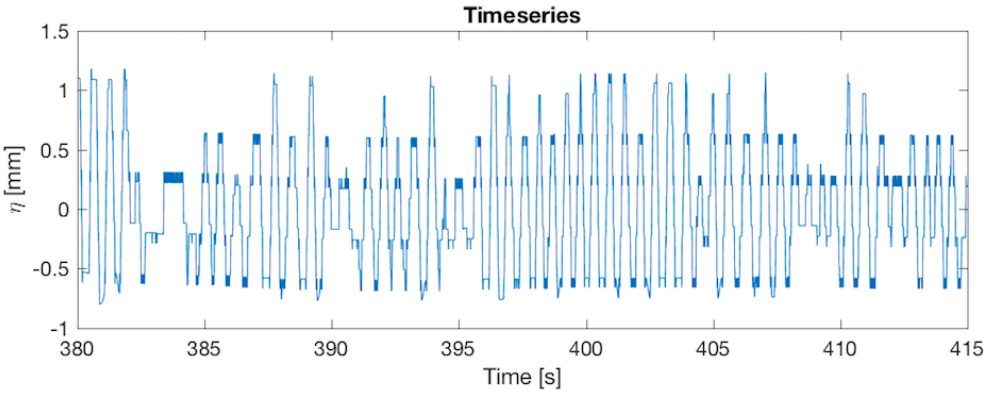

Figure 5.6: Effect of attenuation and stiffness on elastic sheets. Measurements taken at sheet end, location 20

The effect of an high elasticity module must be taken in to consideration when analysing calculated values and statistical properties of the wavefield. Parameters such as significant wave height, characteristic amplitude, kurtosis and skewness could be noticeably influenced by the attenuation as a function of distance into the elastic sheet. The effect of stiffness also increase with increasing thickness of the elastic sheets, resulting in a rapid development at the water-sheet boundary. The effects of elasticity can hence be partitioned into gradual attenuation and rapid attenuation. Gradual attenuation being distance dependent, and rapid attenuation being dependent of elasticity module.

5.2.2.3 Latex sheet

For the Latex sheet, with an E-modul equal to 0.0015 GPa, the effects of stiffness are almost unnoticable. Figure 5.7 shows surface elevation measurements at the beginning of the elastic sheet, and Figure 5.8 shows the surface elevation at the end of the sheet. From the figures it can be observed that attenuation from stiffness mostly affects the low-amplitude waves.

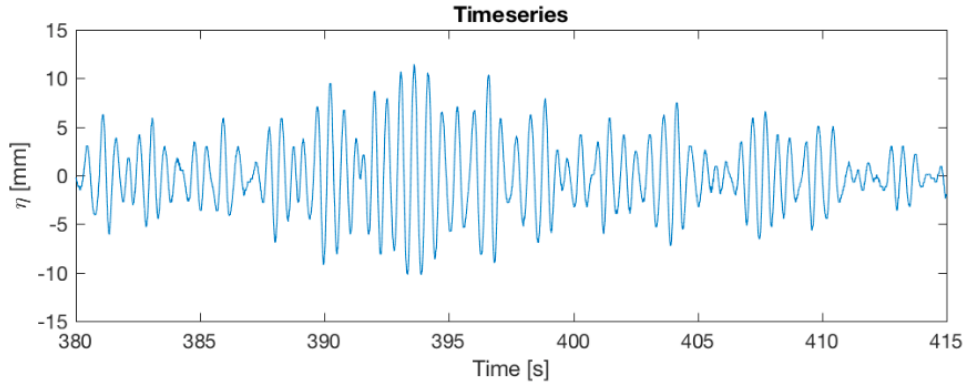

Figure 5.7: Effect of attenuation and stiffness on elastic sheet. Measurements taken at sheet start, location 1

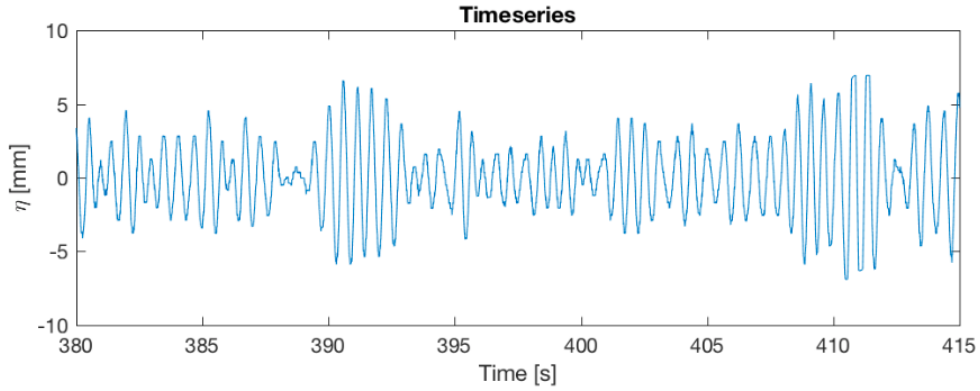

Figure 5.8: Effect of attenuation and stiffness on elastic sheet. Measurements taken at sheet end, location 16

5.2.3 Reflection from elastic sheet

Reflection coefficients are calculated for the open water location (see locations in Figure 5.1) in front of the elastic sheet for all four sheets. This calculation (see Section 3.4) is done to investigate how much of the wavefields energy is transmitted through the boundary between a free surface and a surface covered by an elastic sheet. The coefficient, $\frac{R}{I}$, is calculated between the first and the third probe with a distance of 0.4 m between them. The results are given in Table 5.11 below and are compared to reflection coefficients calculated from reference measurements with a free surface and no sheet in the wave tank shown in Table 5.10.

T_p [s]	Reference measurements
1.1	0.177
1.0	0.187
0.9	0.377

Table 5.10: Reflection coefficient from reference measurements done on a free surface with no sheet in the wave tank.

T_p [s]	R/I - $PEHD_1$	R/I - $PEHD_2$	R/I - $PEHD_3$	R/I - Latex
1.1	0.219	0.161	0.207	0.185
1.0	0.132	0.323	0.188	0.206
0.9	0.494	0.484	0.358	0.355

Table 5.11: Reflection coefficient in front of the elastic sheet for all sheet types used in experiments.

The calculated reflection coefficients calculated show that the reflection of waves at the boundary between free surface and surface covered by an elastic sheet is more dominating for the wavefield with low peak period, $T_p = 0.9$ s. Reflection increases as the peak period and angular frequency of the waves increases. The Latex sheet gives the least reflection, hence it shows the lowest reflection coefficients.

5.2.4 Wave phase speed and group velocity

To investigate wave propagation inside the elastic sheets wave phase speed c_p and group velocity c_g are calculated from equations (3.54) and (3.55) in Section 3.3.6.

5.2.4.1 $PEHD_1$

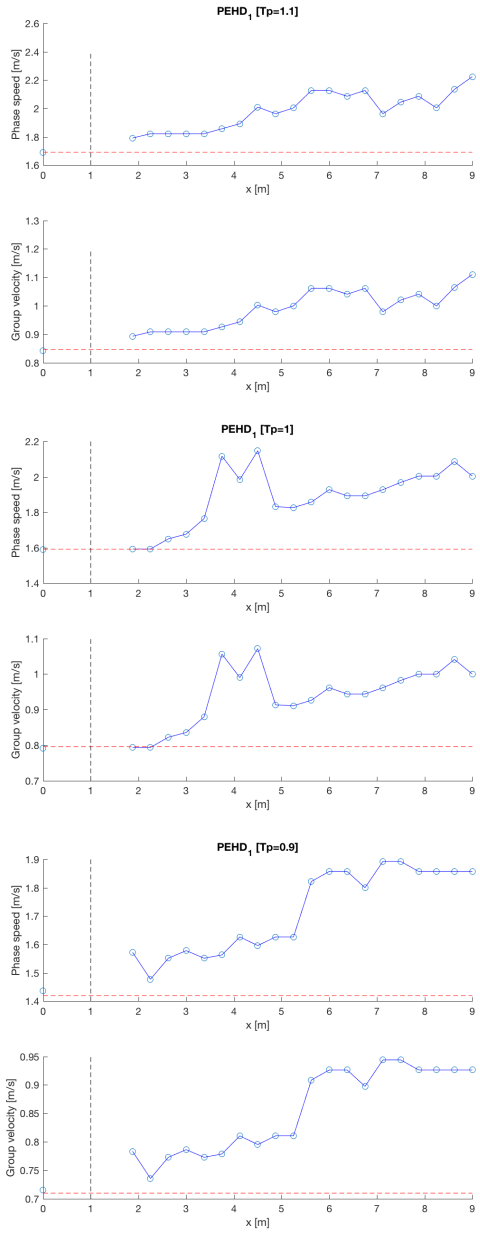

Figure 5.9: Phase speed and group velocity as a function of spatial distance for PEHD sheet with 1 mm thickness for $T_p = 1.1,\ 1.0,\ 0.9$ s

5.2.4.2 $PEHD_2$

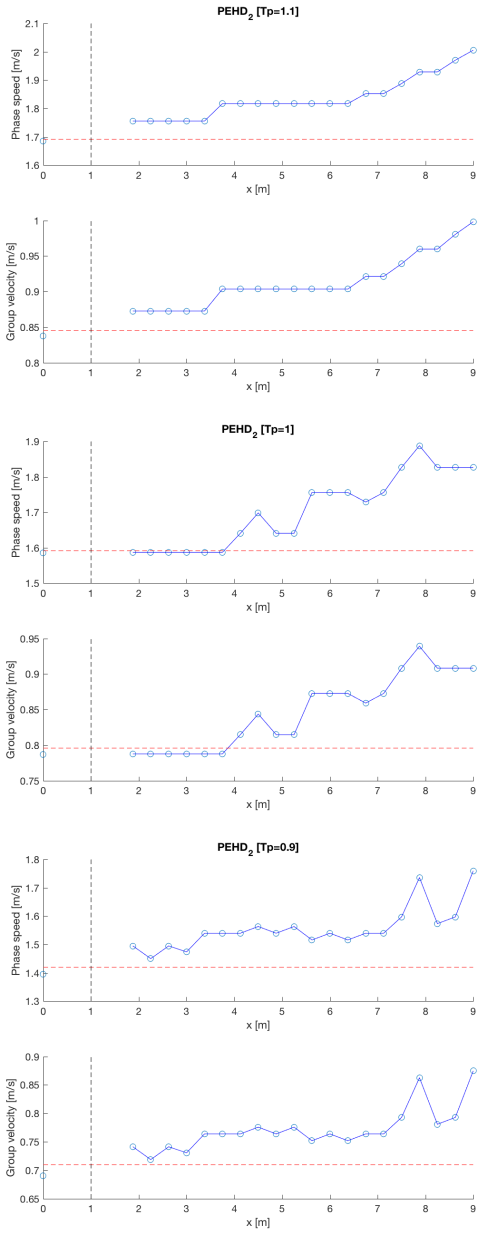

Figure 5.10: Phase speed and group velocity as a function of spatial distance for PEHD sheet with 2 mm thickness for $T_p = 1.1,\ 1.0,\ 0.9$ s

5.2.4.3 $PEHD_3$

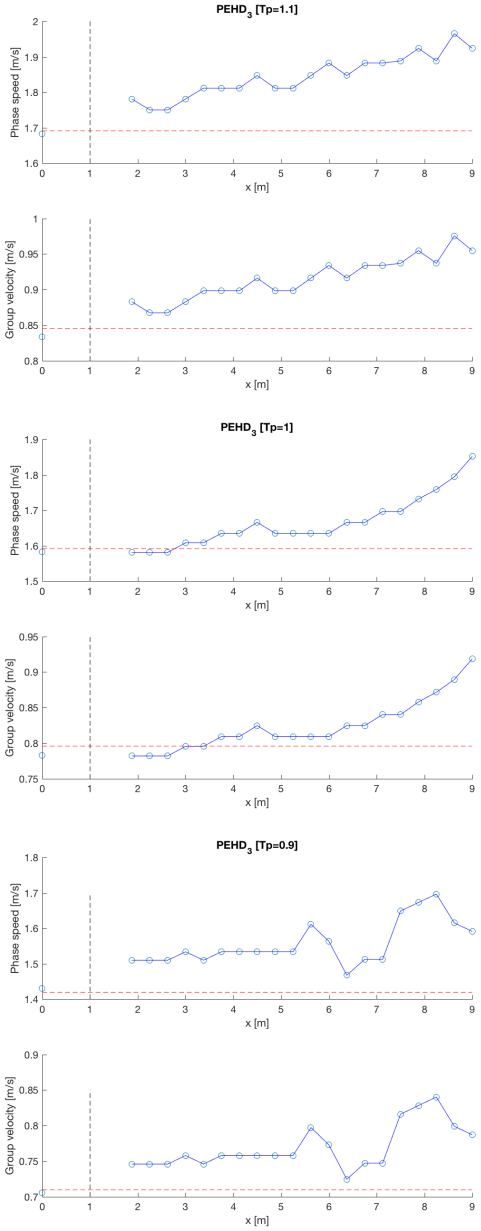

Figure 5.11: Phase speed and group velocity as a function of spatial distance for PEHD sheet with 3 mm thickness for $T_p = 1.1,\ 1.0,\ 0.9$ s

5.2.4.4 Latex

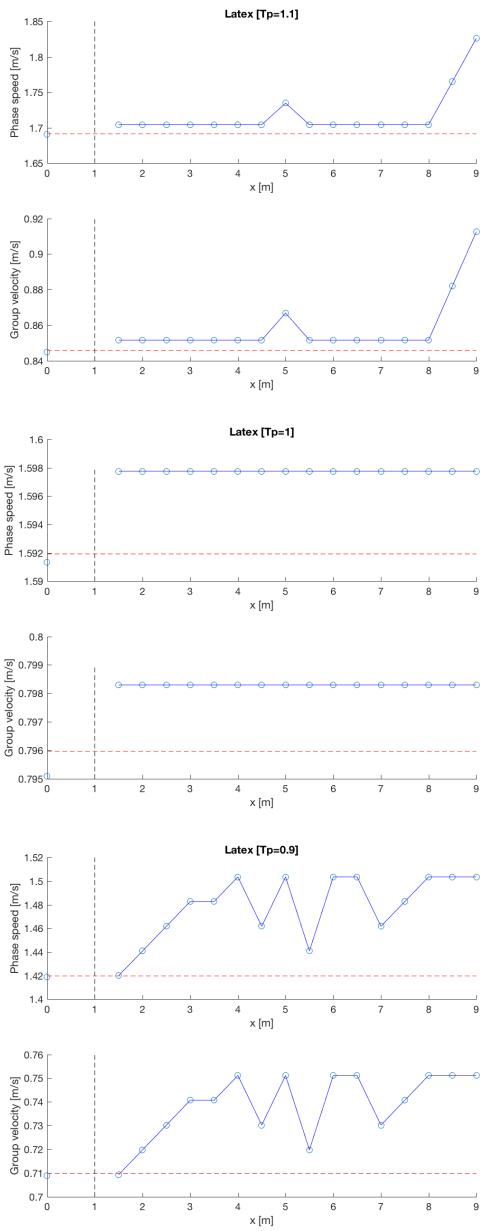

Figure 5.12: Phase speed and group velocity as a function of spatial distance for Latex sheet with 0.2 mm thickness for $T_p = 1.1,\ 1.0,\ 0.9$ s

From the results it can be observed that both the phase speed and the group velocity gradually increase as the waves propagate into the elastic sheets. For all sheet types, c_p and c_g lie above the reference measurement line (red dashed line). Speed c_p and velocity c_g decrease as a function of thickness and peak period T_p and the group velocity seems to be approximately half the phase speed for all sheet types. The values of wave phase speed and group velocities are slightly lower inside the Latex sheet than they are inside the PEHD sheets.

5.2.5 Amplitude attenuation

To study the attenuation of amplitudes of the wavefield the characteristic amplitudes, a_c, are plotted as a function of distance x in the wave tank. Following *Sutherland et.al* the characteristic amplitudes are compared to theoretical values as the exponential decay is described to follow the attenuation curve given by:

$$a(x) = a_0 e^{-(\beta\sqrt{\frac{\omega}{2\beta}}(\frac{1}{sinh2kH}+\frac{1}{kB})k/c_g)x} \tag{5.1}$$

5.2.5.1 PEHD$_1$

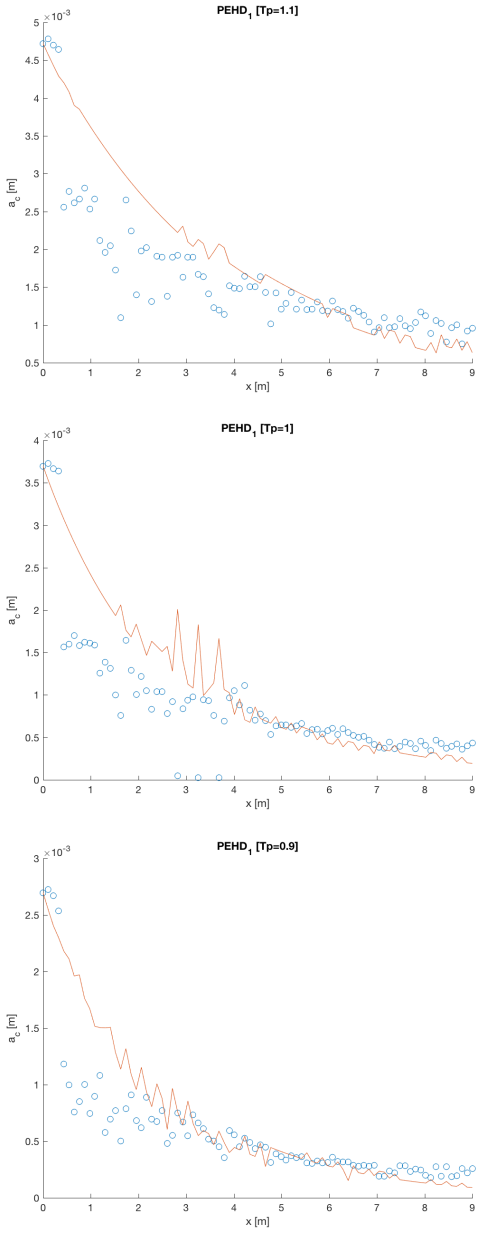

Figure 5.13: Amplitude attenuation as a function of spatial distance for PEHD sheet with 1 mm thickness for T_p = 1.1, 1.0, 0.9 s

5.2.5.2 PEHD$_2$

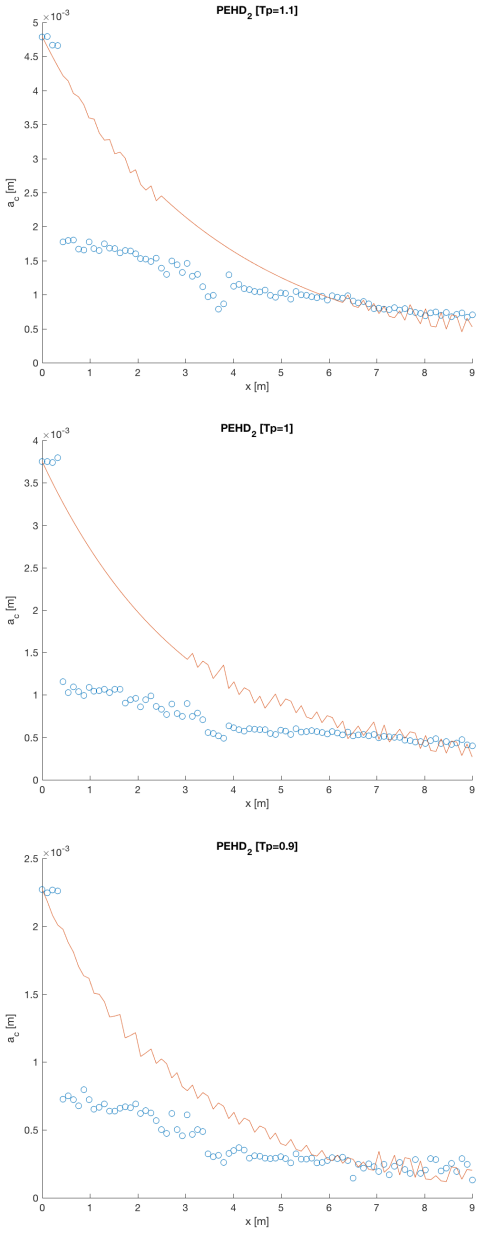

Figure 5.14: Amplitude attenuation as a function of spatial distance for PEHD sheet with 2 mm thickness for T_p = 1.1, 1.0, 0.9 s

5.2.5.3 $PEHD_3$

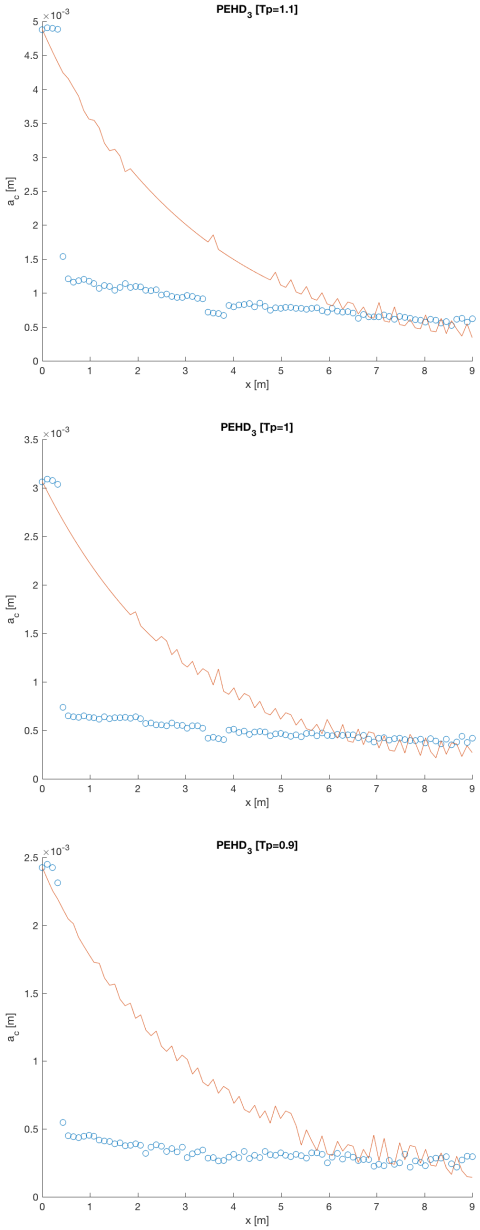

Figure 5.15: Amplitude attenuation as a function of spatial distance for PEHD sheet with 3 mm thickness for T_p = 1.1, 1.0, 0.9 s

5.2.5.4 Latex

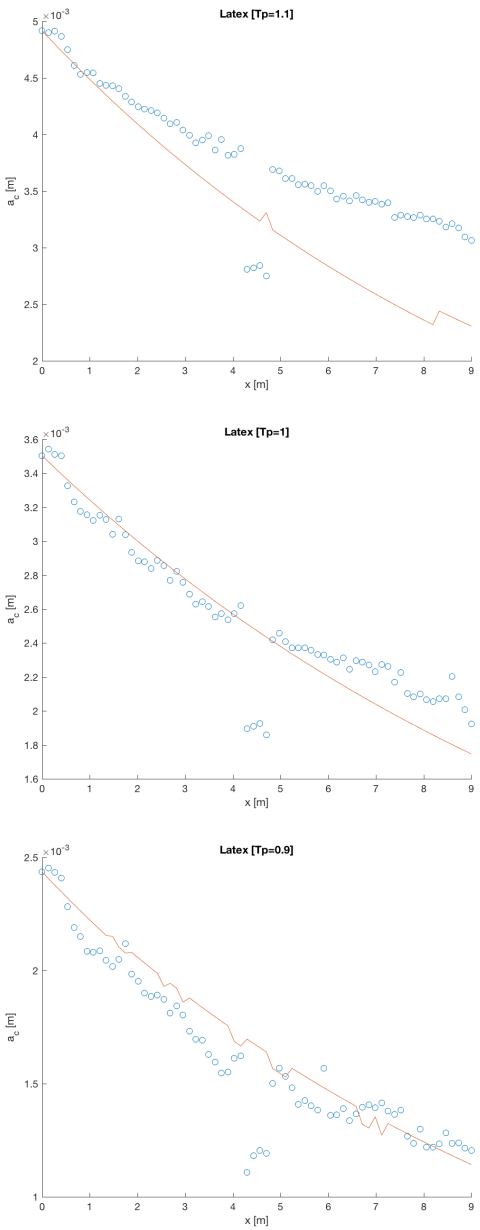

Figure 5.16: Amplitude attenuation as a function of spatial distance for Latex sheet with 0.2 mm thickness for T_p = 1.1, 1.0, 0.9 s

Theoretical attenuation curve is represented as the red curve in all the plots, where kinematic viscosity β is adjujsted to fit the measured data (see Table 5.4). It should be taken into consideration that *Sutherland et.al* have concluded that the given function for amplitude attenuation should include elasticity of the sheet covering the surface, but is still not included here. From the figures it can be observed that the energy intensity decreases exponentially as waves propagate into the elastic sheets. The decrease in energy is much bigger and rapid for the PEHD sheets than for the Latex sheet.

5.2.6 Skewness and kurtosis

The statistical parameters skewness and kurtosis are calculated using the MatLab functions *skewness* and *kurtosis*, respectively. It should be mentioned that for the PEHD sheets the waves are stongly attenuated and the energy intensity is approximately zero at the end of the sheets, therefore the values are calculated as the mean values of skewness and kurtosis for each location.

5.2.6.1 $PEHD_1$

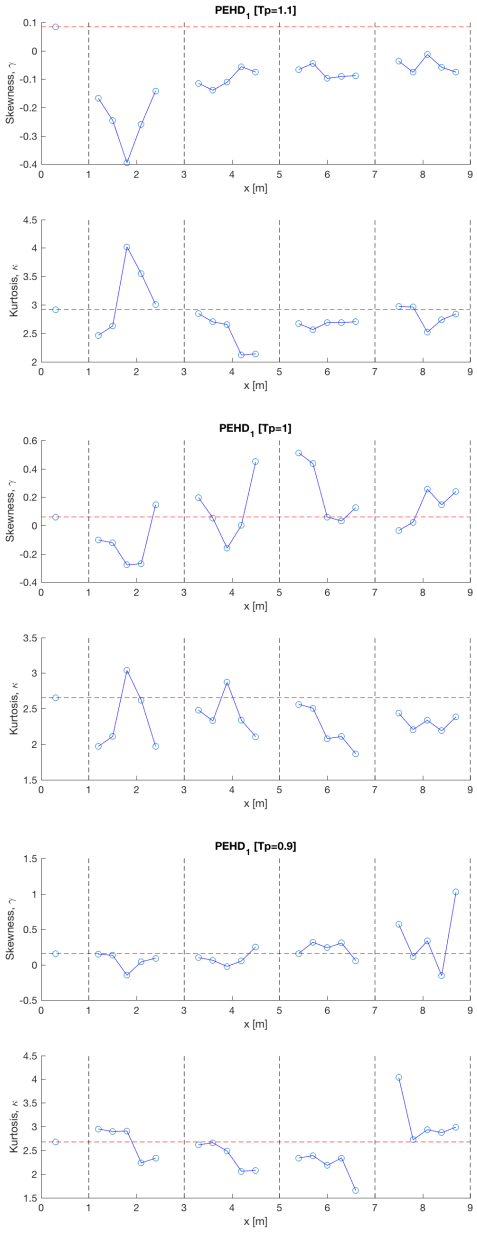

Figure 5.17: Skewness and kurtosis as a function of spatial distance for PEHD sheet with 1 mm thickness for T_p = 1.1, 1.0, 0.9 s

5.2.6.2 $PEHD_2$

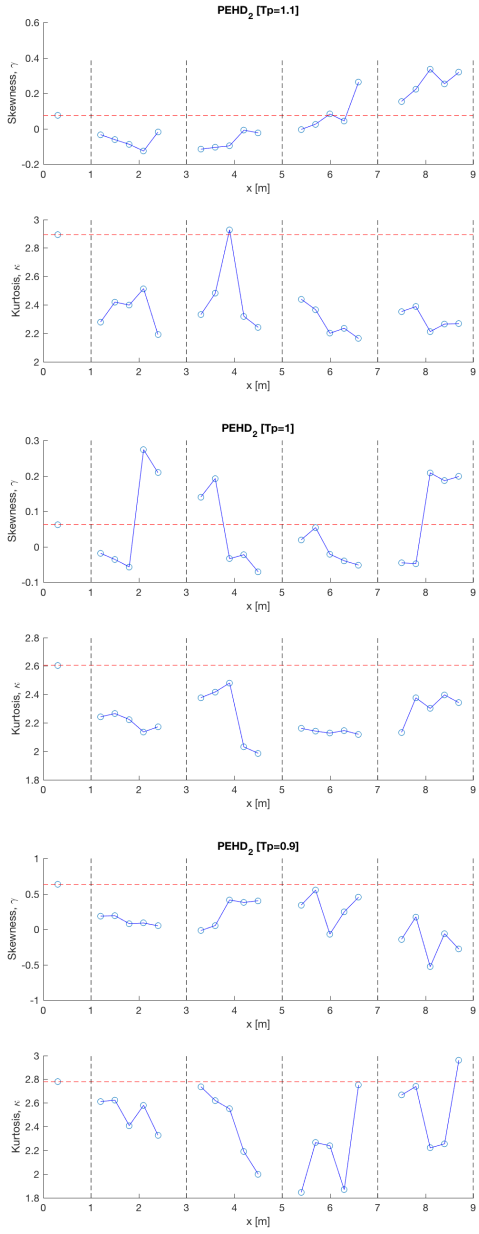

Figure 5.18: Skewness and kurtosis as a function of spatial distance for PEHD sheet with 2 mm thickness for T_p = 1.1, 1.0, 0.9 s

5.2.6.3 $PEHD_3$

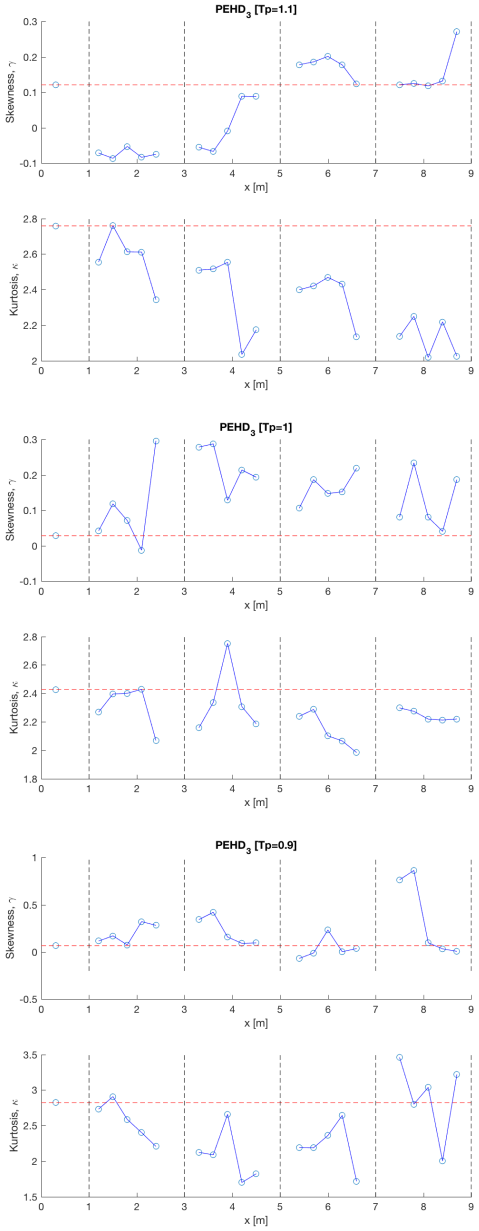

Figure 5.19: Skewness and kurtosis as a function of spatial distance for PEHD sheet with 3 mm thickness for T_p = 1.1, 1.0, 0.9 s

5.2.6.4 Latex

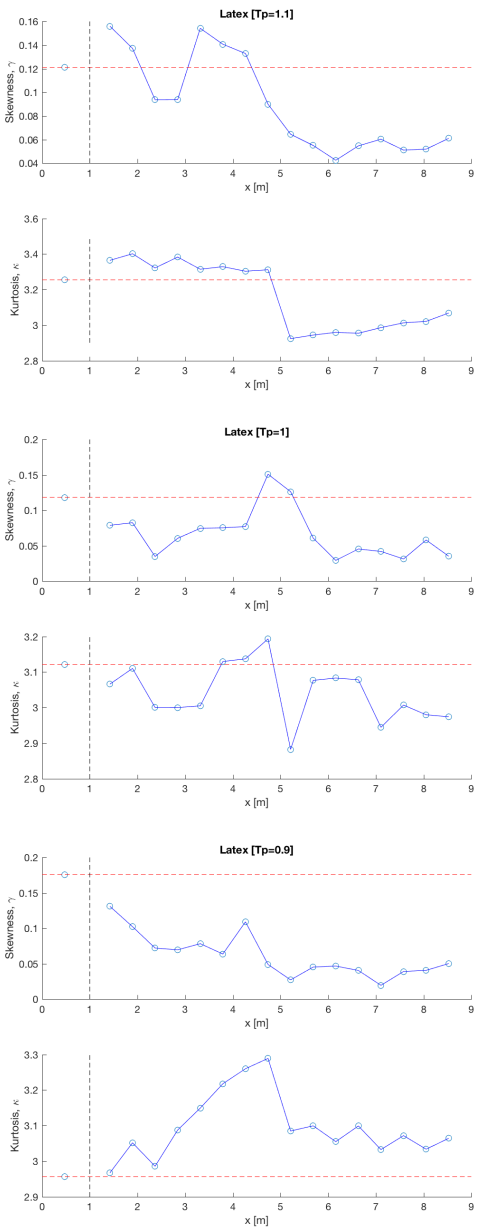

Figure 5.20: Skewness and kurtosis as a function of spatial distance for Latex sheet with 0.2 mm thickness for T_p = 1.1, 1.0, 0.9 s

Reference measurements on free surface in front of elastic sheet, represented by the red dashed line, is added to all plots (Fig.5.17-5.20). Plots of skewness γ and kurtosis κ as a function of distance in the wave tank show how the wavefield develops in statistical terms. Plots of skewness γ shows sligthly oscillating values for all sheets. For $PEHD_1$ and $PEHD_3$ with $T_p = 0.9s$ one can observe a calculated skewness of 1.0, this is the maximum calculated skewness for all sheets. For the Latex sheet calculated skewness lies between a maximum of 0.16 and a minimum of 0.002.

From the values of kurtosis it can be observed that measurements on sheet $PEHD_1$ have a peak in kurtosis for peak period $T_p = 1.1$ s and 1.0 s at approximately 1 meter into the sheet. For $T_p = 0.9s$ the peak kurtosis is found at the end of the elastic sheet. For $PEHD_2$ one can also observe the peak kurtosis at 1 meter into the sheet for $T_p = 1.0$ s, but not for the two other peak periods. It is also observed that the calculated kurtosis values decrease as thickness of the PEHD sheets increase. For the Latex sheet the kurtosis κ seems to be increasing as waves propagates into the Latex sheet, but from approximately 5 meters the values start decreasing.

5.2.7 Power spectral density

The power spectral density is calculated using *pwelch* function in MatLab, with a 50% overlap and windows of 1000 values for each calculation. This function returns the power spectral density (PSD) estimate of the input signal using Welch's overlapped segment averaging estimator. Since the surface elevation of four probes is a matrix PSD is computed independently for each column and the result is the one-sided power spectral density estimate of the surface elevation.

5.2.7.1 $PEHD_1$

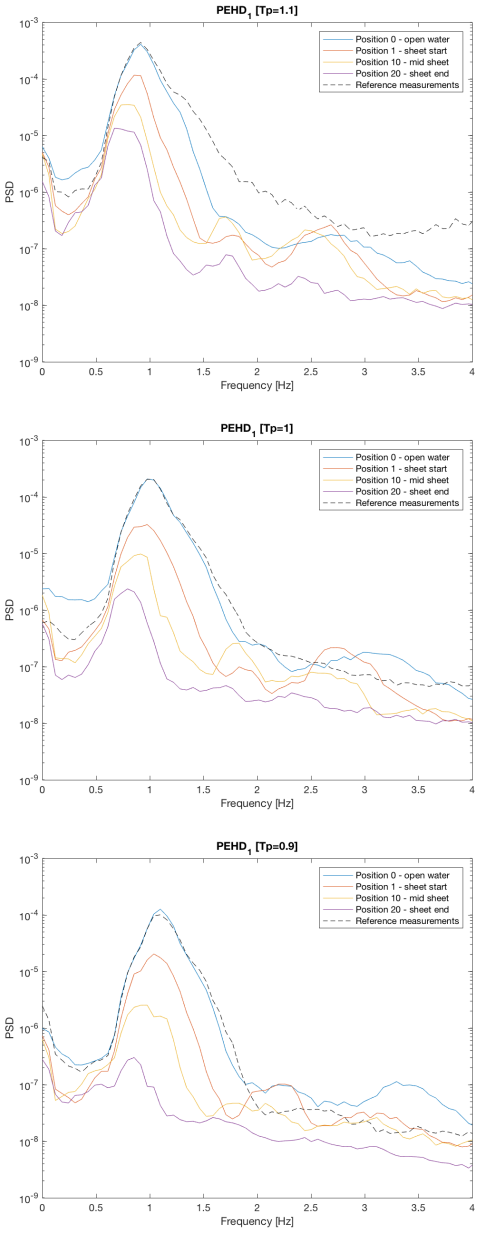

Figure 5.21: Power spectral density for PEHD sheet with 1 mm thickness for $T_p = 1.1,\ 1.0,\ 0.9$ s

5.2.7.2 $PEHD_2$

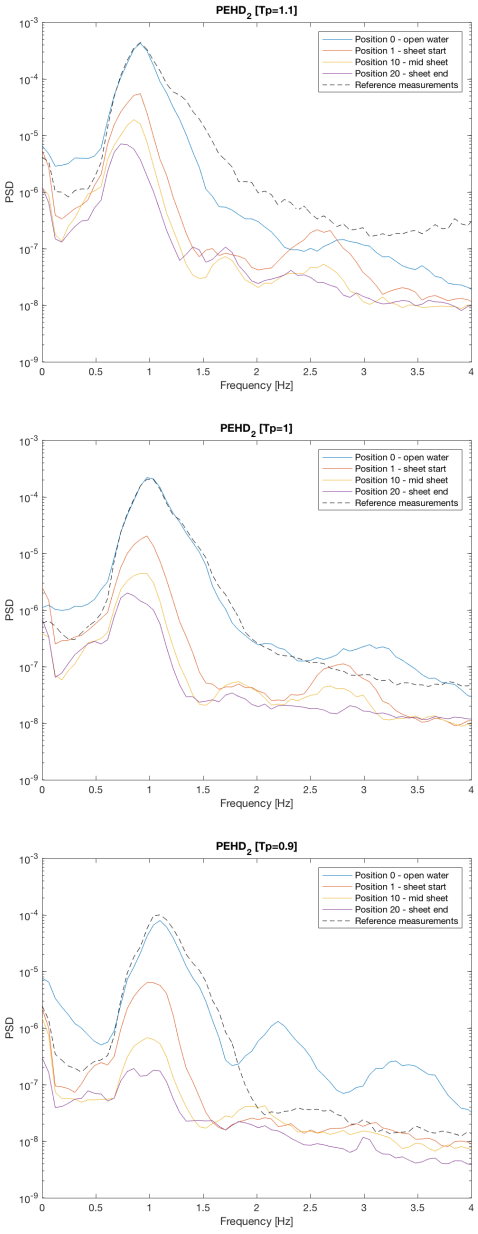

Figure 5.22: Power spectral density for PEHD sheet with 2 mm thickness for $T_p = 1.1,\ 1.0,\ 0.9$ s

5.2.7.3 $PEHD_3$

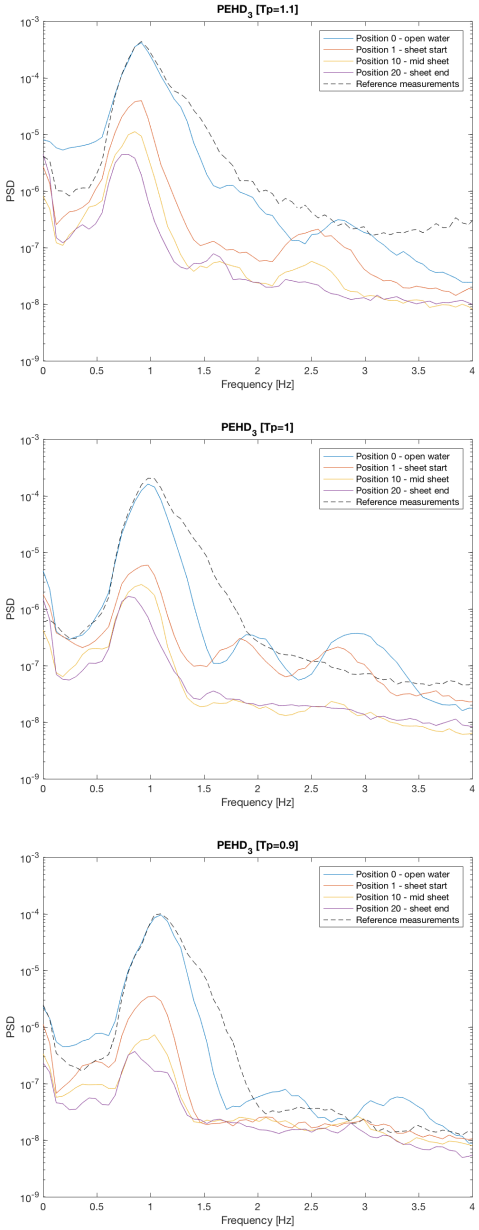

Figure 5.23: Power spectral density for PEHD sheet with 3 mm thickness for $T_p = 1.1,\ 1.0,\ 0.9$ s

5.2.7.4 Latex

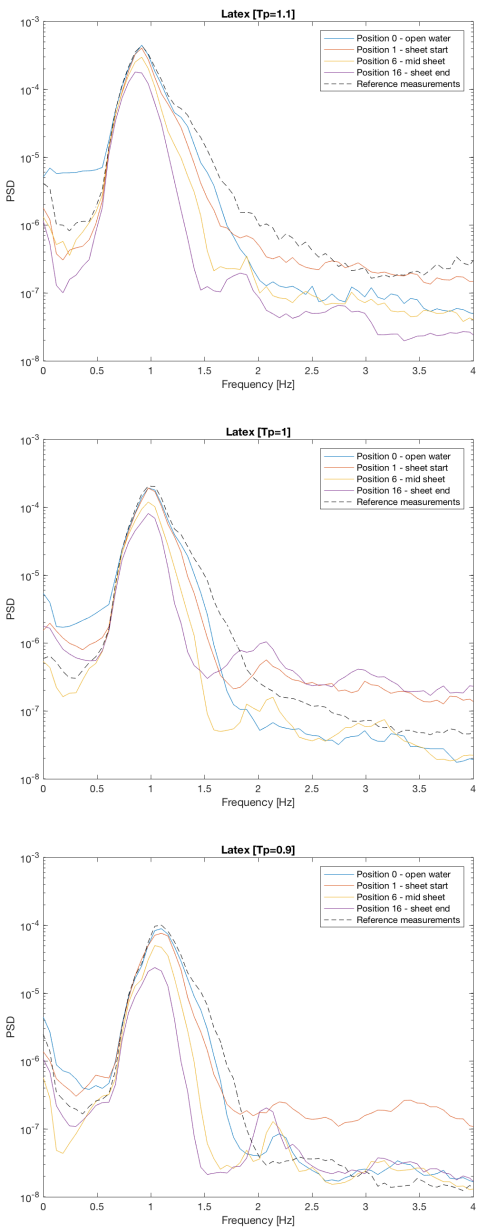

Figure 5.24: Power spectral density for Latex sheet with 0.2 mm thickness for $T_p = 1.1,\ 1.0,\ 0.9$ s

From the figures, Fig. 5.21-5.24 it can be observed that attenuation of waves is a function of both sheet thickness and peak period. The attenuation of waves increase as the thickness increase and peak period T_p decrease. Therefore the waves are mostly affected by attenuation for sheet $PEHD_3$ and $T_p = 0.9$ s. The least attenuated waves are found for the Latex sheet with $T_p = 1.1$ s. In addition to attenuation it can also be observed that the peak frequency f_p tends towards lower values as the wavefield propagates into all elastic sheets.

5.2.8 Wavenumber-frequency spectrum

For all sheets the wavenumber-frequency spectrum is calculated using the two-dimensional Fourier transform. The spectrum provides information and visibility of linear- and non-linear effects of the wavefield in terms of conformity with the dispersion relation. Because of aliasing of the signals the spectrum needed to be rearranged [24]. For the PEHD sheets, the energy intensity of linear effects are not visible because of the highly attenuated time series of waves from the middle to the end of the elastic sheet. The spectrum is plotted as a function of (k, ω) with the dispersion relation curve to illustrate linear effects and its harmonics. The non-linear effects arise as we plot the spectrum with logarithmic scale as shown in the plots with dB colorbar. Both linear and logarithmic scaled plots show the energy intensity of the wave distribution.

5.2.8.1 Aliasing

Plots of the wave spectrums as a function of (k, ω) show a clear aliasing effect of the signals in the spatial domain. Figure 5.25 and 5.26 below show the linear and logarithmic scaled plots of the (k, ω)-spectrums with the aliasing effect of signals. This effect is later removed and the de-aliased spectrum is retrieved for both cases. The red lines, representing $n\Delta k$ where $n = 1, 2, 3, \ldots$ calculated from $\frac{2\pi}{L}$ where L is the measuring length in x-direction, are the measurement grid.

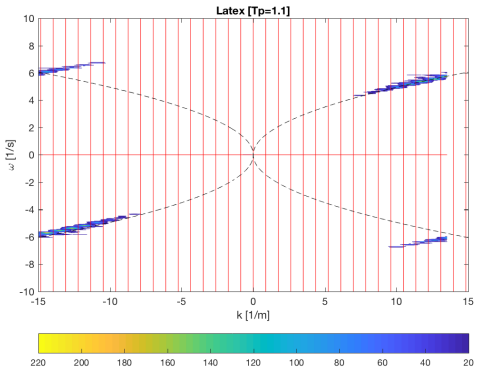

Figure 5.25: Linear scaled spectrum plot with aliasing for Latex sheet with 0.2 mm thickness for $T_p = 1.1$ s. Black dashed line shows dispersion relation for elastic sheet.

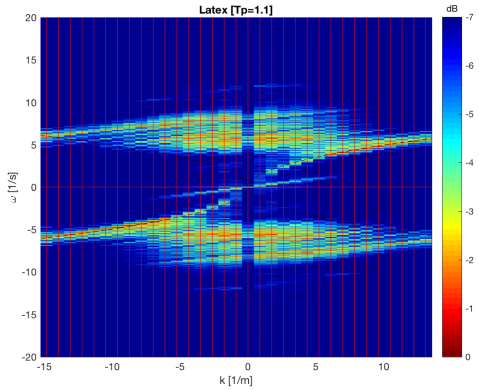

Figure 5.26: Logarithmic scaled spectrum plot with aliasing for Latex sheet with 0.2 mm thickness for $T_p = 1.1$ s. Black dashed line shows dispersion relation and its harmonics for elastic sheet.

The grid-lines, or reconstruction lines, show the grid in the spatial domain. To retrieve the de-aliased spectrum, values are replaced from negative wavenumbers k to continue the values of the spectrum at the positive wavenumbers, making the spectrum to be periodic. This means that the entire part of the spectrum ranging from zero to the minimum wavenumber, is replaced to the maximum wavenumber extending the spectrum to be able to investigate effects of the wavefield. This principle is used for both the linear and logarithmic scaled plots.

5.2.8.2 Free surface reference measurements

As earlier mentioned reference measurements are taken on a free surface with no elastic sheet in the tank. The reference measurements are processed in the same way, hence taking the two-dimensional Fourier transform of the surface elevation, as for the measurements taken on the elastic sheet. It should be noted that the spatial resolution is much worse for the free surface measurements than for the elastic sheets, as these measurements are taken from only four probes, hence one location.

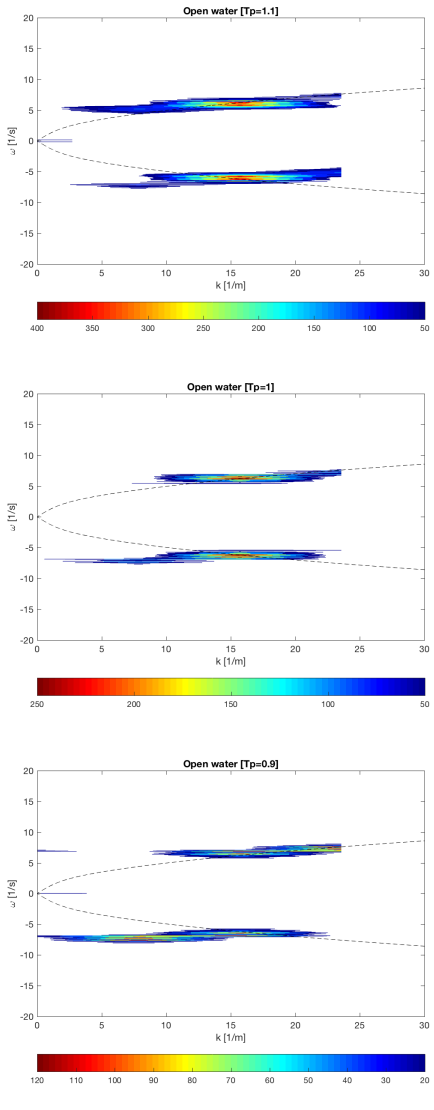

Figure 5.27: Linear scaled spectrum plot for open water with $T_p = 1.1, 1.0, 0.9$ s. Black dashed line shows dispersion relation for gravity waves.

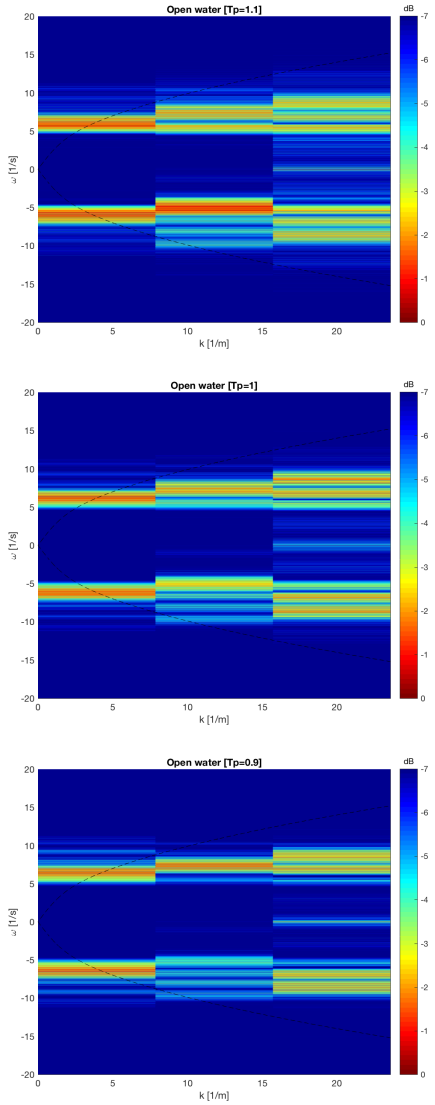

Figure 5.28: Logarithmic scaled spectrum plot for open water with $T_p = 1.1, 1.0, 0.9$ s. Black dashed line shows dispersion relation for gravity waves.

5.2.8.3 Linear effects

Plot of the linear scaled wavenumber-frequency spectrum shows if the linear dispersion relation is fulfilled for waves in the elastic sheets. For some of the peak periods with the PEHD sheets the waves are highly attenuated, especially low peak period T_p, which can be observed in the figures below.

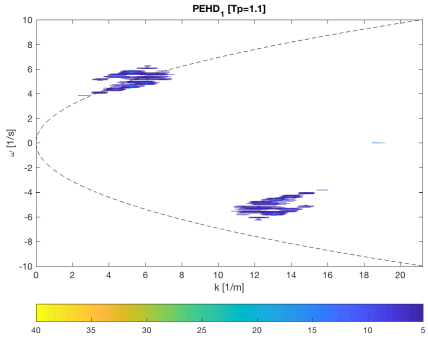

Figure 5.29: Linear scaled spectrum plot for PEHD sheet sheet with 1 mm thickness for $T_p = 1.1, 1.0, 0.9$ s. Black dashed line shows dispersion relation for elastic sheet.

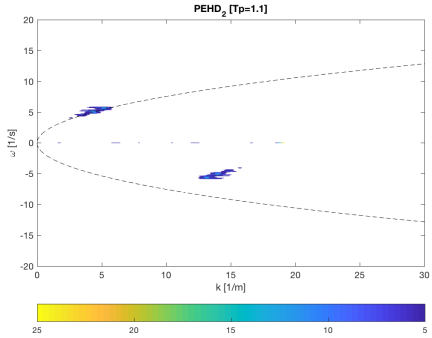

Figure 5.30: Linear scaled spectrum plot for Latex sheet with 2 mm thickness for $T_p = 1.1, 1.0, 0.9$ s. Black dashed line shows dispersion relation for elastic sheet.

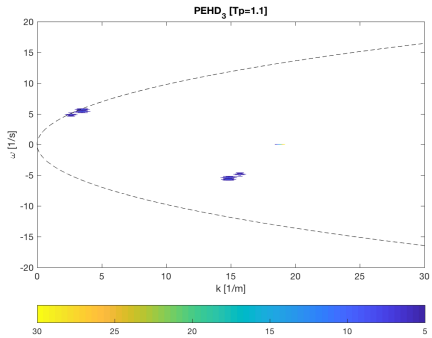

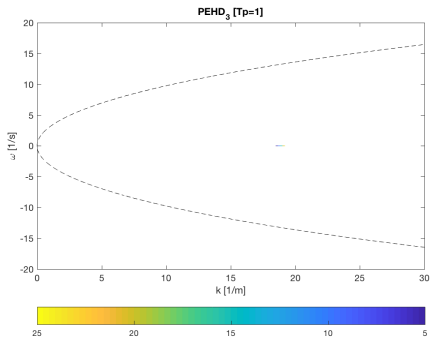

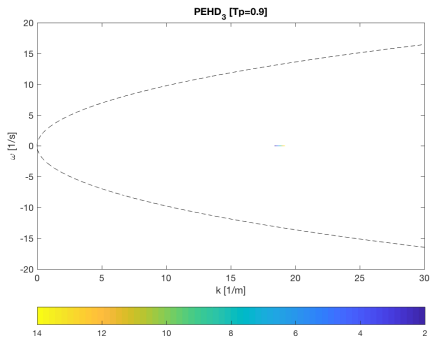

Figure 5.31: Linear scaled spectrum plot for PEHD sheet sheet with 3 mm thickness for $T_p = 1.1, 1.0, 0.9$ s. Black dashed line shows dispersion relation for elastic sheet.

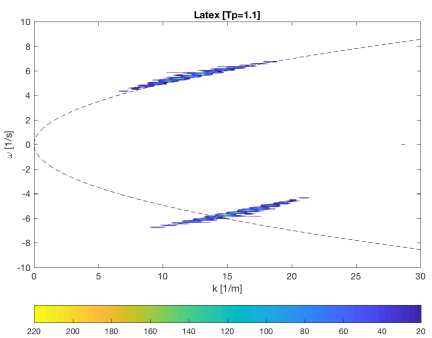

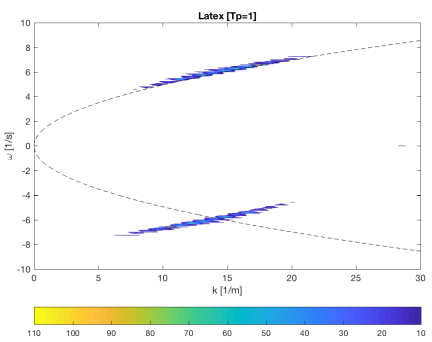

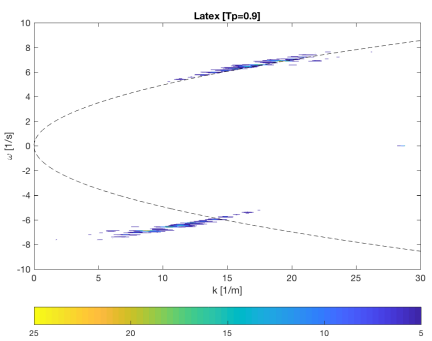

Figure 5.32: Linear scaled spectrum plot for Latex sheet with 0.2 mm thickness for $T_p = 1.1, 1.0, 0.9$ s. Black dashed line shows dispersion relation for elastic sheet.

The plot of energy intensity in Latex sheet shows a clear linear relation as energy intensities are located around the dispersion relation curve. As peak period T_p decreases the energy intensity tend towards higher wavenumbers k. For PEHD_1 the energy has a more cloudly distribution. Energy is distributed over a larger angular frequency range, and shows the same trend as the Latex sheet for decreasing peak period. For all PEHD sheets with $T_p = 0.9$ s the two-dimensional spectrum does not show any energy intensity.

5.2.8.4 Non-linear effects

To investigate non-linear effects of the wavenumber-frequency spectrum the spectrum is plotted with logarithmic scale. The spectrum is firstly made dimensionless as $10\log(\frac{S}{S_{max}})$ and then plotted as a function of (k, ω). The plot then shows the relative energy intensity in decibell (dB) of the waves for given (k, ω) values. Linear dispersion relation and its harmonics are plotted as (k, ω), $(2k, 2\omega)$ and $(3k, 3\omega)$, respectively, as black dashed lines in the plots [26].

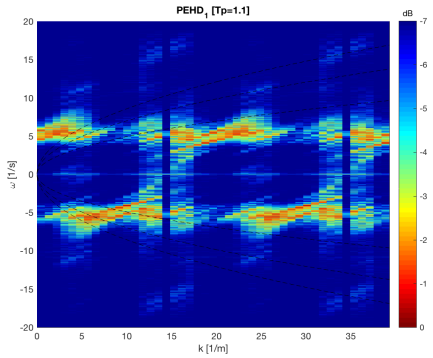

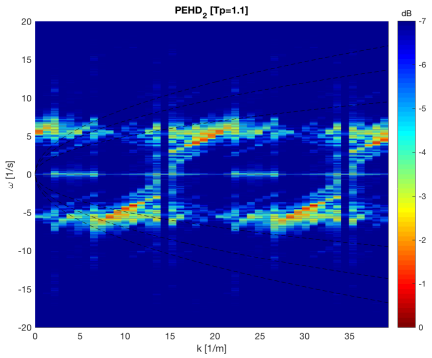

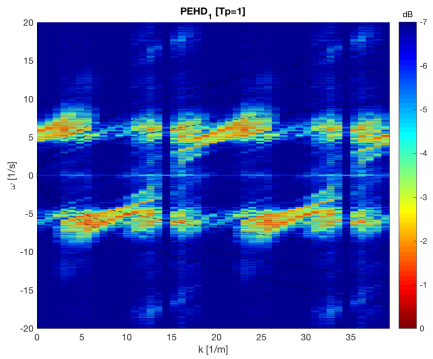

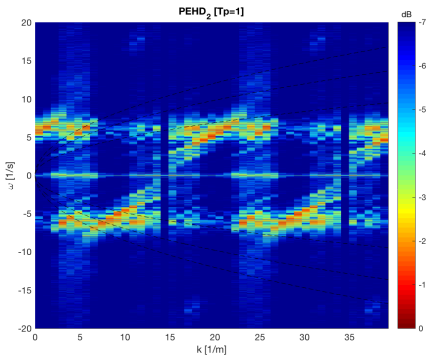

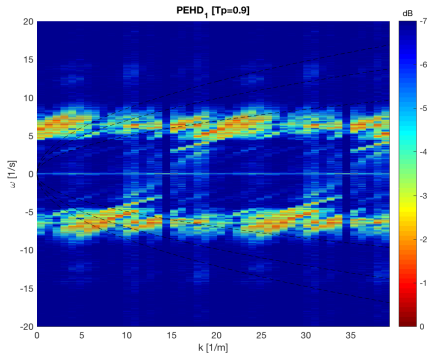

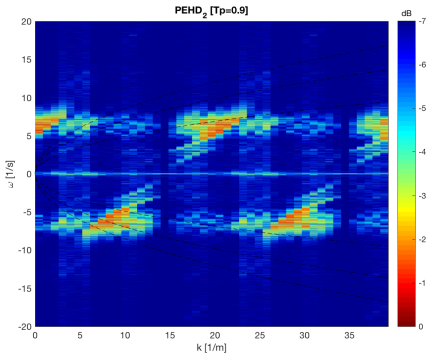

Figure 5.33: Logarithmic scaled spectrum plot for PEHD sheet sheet with 1 mm thickness for $T_p = 1.1, 1.0, 0.9$ s. Black dashed line shows dispersion relation and its harmonics up to the third order.

Figure 5.34: Logarithmic scaled spectrum plot for PEHD sheet with 2 mm thickness for $T_p = 1.1, 1.0, 0.9$ s. Black dashed line shows dispersion relation and its higher harmonics up to third order.

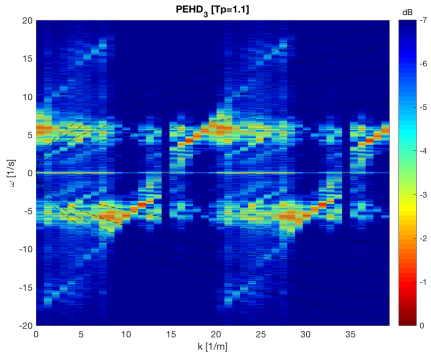

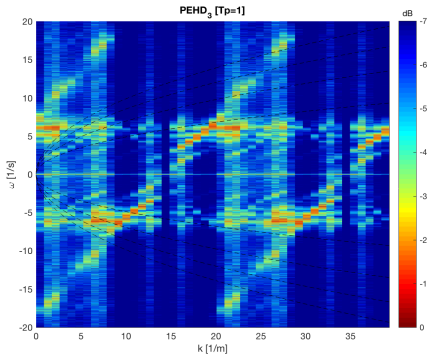

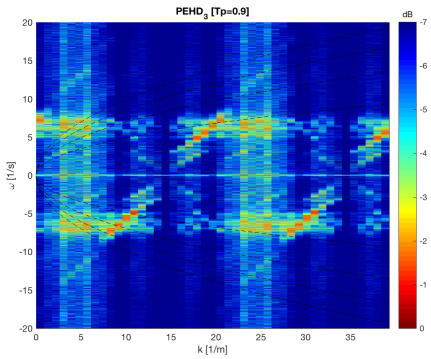

Figure 5.35: Logarithmic scaled spectrum plot for PEHD sheet sheet with 3 mm thickness for $T_p = 1.1, 1.0, 0.9$ s. Black dashed line shows dispersion relation and its higher harmonics up to fourth order.

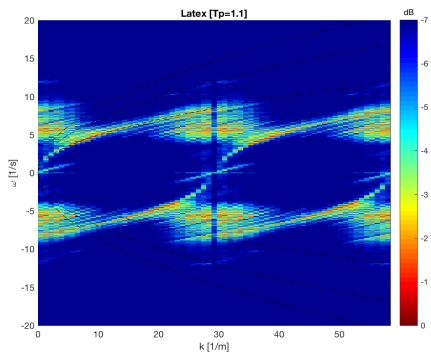

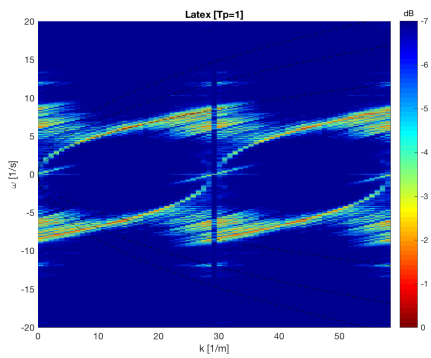

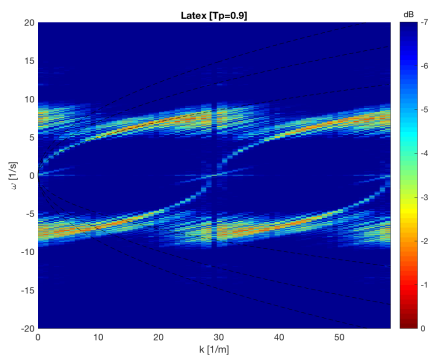

Figure 5.36: Logarithmic scaled spectrum plot for Latex sheet with 0.2 mm thickness for $T_p = 1.1, 1.0, 0.9$ s. Black dashed lines shows linear dispersion relation and its harmonics up to the third order.

One can observe from the spectrum plots above that the resolution in space is worse for PEHD sheets than for the Latex sheet. For the Latex sheet the most of the energy is located along the first harmonic (k, ω), but there are relative intensities from the zeroth and second harmonic to be found as well. For the PEHD sheets the relative energy intensity along the first harmonic is to be found at higher wavenumbers k than for the Latex sheet. It also seems as the relative energy intensity is distributed over a larger angular frequency interval for PEHD sheets, and the size of the interval is a function of thickness.

5.2.9 BFI

The Benjamin-Feir Index (BFI) is often used to indicate instability of the wavefield. The BFI is, as earlier mentioned, the ratio between steepness and bandwidth of the measured surface elevation (2.33). BFI is plotted as a function of spatial distance for each sheet, where mean values are calculated from four probe measurements for each location.

5.2.9.1 PEHD$_1$

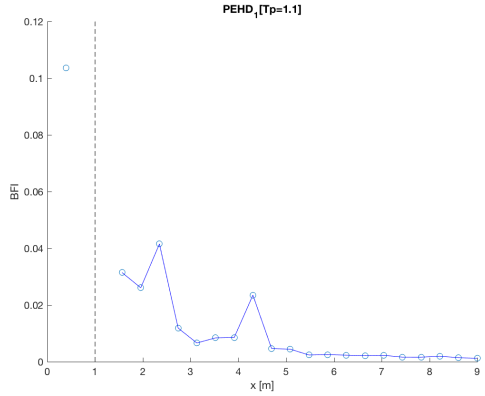

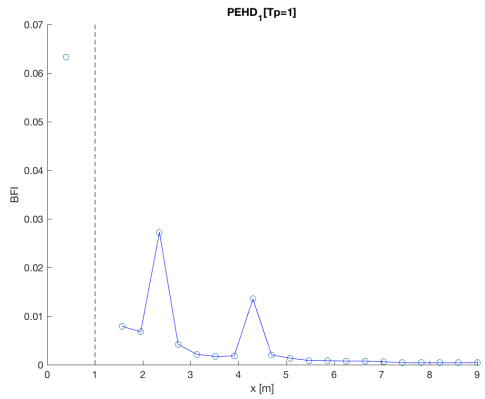

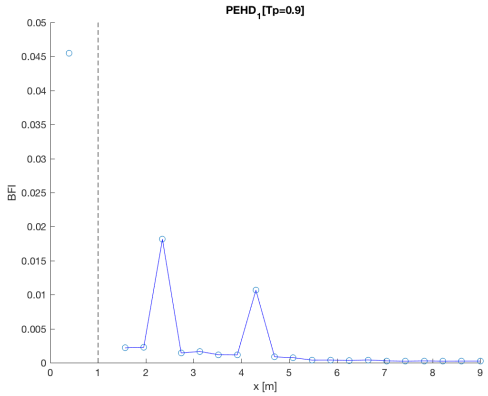

Figure 5.37: Benjamin-Feir index (BFI) for PEHD sheet with 1 mm thickness for $T_p = 1.1,\ 1.0,\ 0.9$ s

5.2.9.2 PEHD$_2$

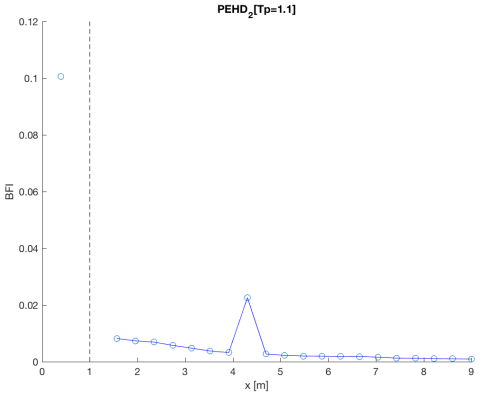

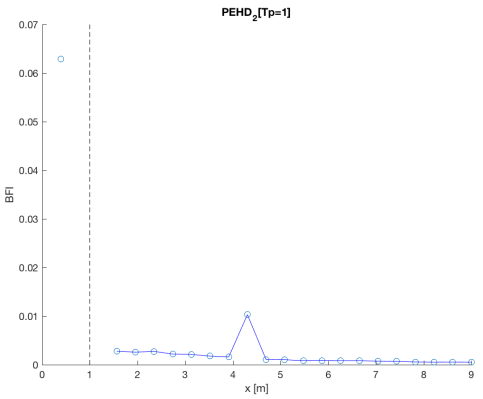

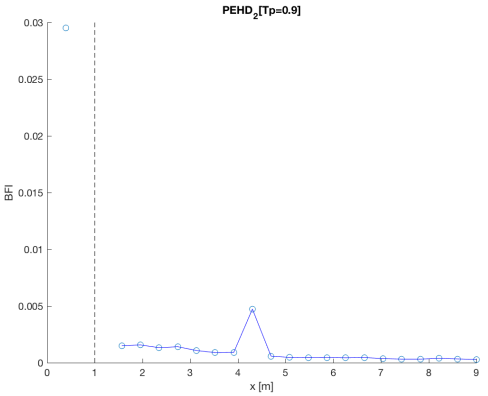

Figure 5.38: Benjamin-Feir index (BFI) for PEHD sheet with 2 mm thickness for $T_p = 1.1,\ 1.0,\ 0.9$ s

5.2.9.3 PEHD$_3$

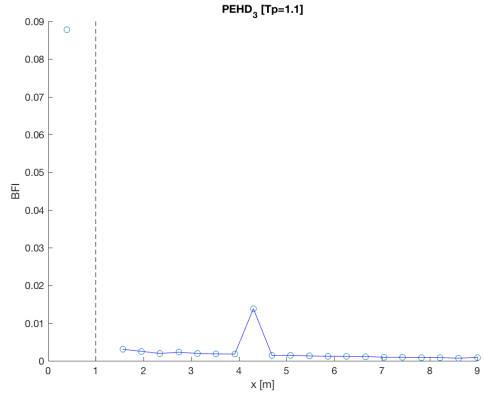

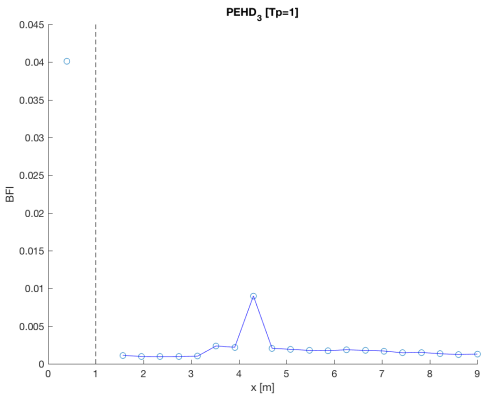

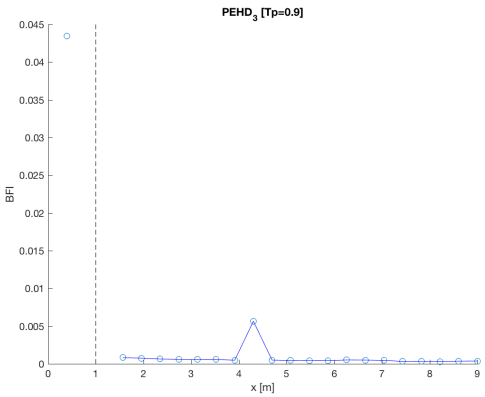

Figure 5.39: Benjamin-Feir index (BFI) for PEHD sheet with 3 mm thickness for $T_p = 1.1,\ 1.0,\ 0.9$ s

5.2.9.4 Latex

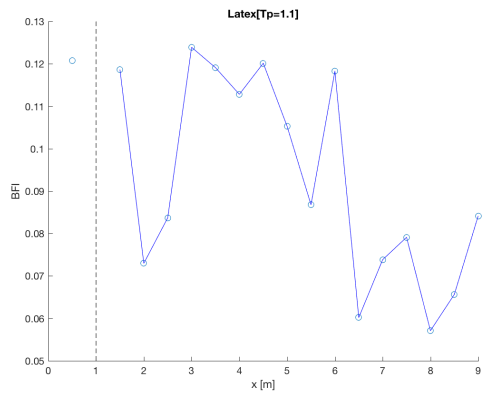

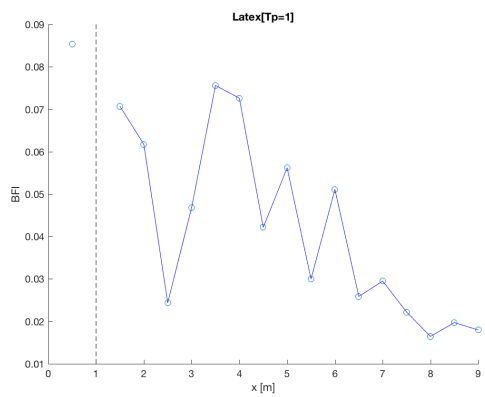

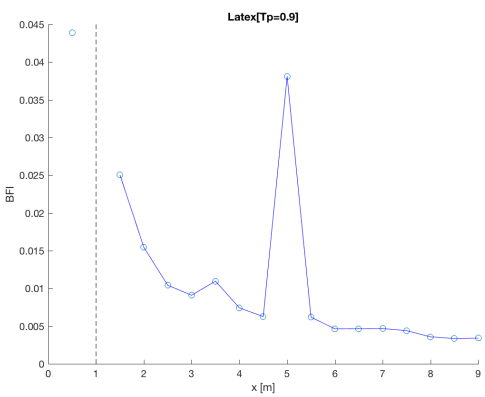

Figure 5.40: Benjamin-Feir index (BFI) for Latex sheet with 0.2 mm thickness for $T_p = 1.1,\ 1.0,\ 0.9$ s

Calculations of Benjamin-Feir Index for PEHD sheets show an exponential decay as a function of distance, and that the wavefield tends to develop towards a more stable state inside the elastic sheets as the calculated values decrease. For the PEHD$_1$ sheet there can be observed a very small local instability at 2.5 and 4.5 meters for all peak periods. For PEHD$_2$ and PEHD$_3$ the local instability is only found at 4.5 meters for both sheet types. The amount of instabilities increase for the Latex sheet, and is hence showing a maximum BFI of 0.12 inside the elastic sheet.

Chapter 6

Discussion

This chapter contains discussions of the experimental results presented in Chapter 5, and is divided into six sections. The first section gives a discussion on the tables of wave characteristics, and the second section discusses the reflection at the front of the elastic sheets. The third and fourth section discusses calculated skewness and kurtosis, phase speed and group velocity, respectively. In the fifth section wave attenuation is discussed and in the sixth section the discussion on non-linear effects is contained.

6.1 Wave characteristics

As mentioned in Chapter 5, Section 5.2.1, the results of wave propagation into an elastic cover are gradually decreased peak frequency in addition to decreasing wavenumber. Decreasing wavenumber means that the wavefield consists of longer waves inside the elastic sheets than on open water, and that shorter waves are more exposed to attenuation. The transition from a wavefield dominated by shorter waves to a wavefield dominated by longer waves happens gradually as waves propagate further into the elastic sheets, and wavelength increases as a function of distance. Significant waveheight and characteristic amplitude decrease drastically when the surface environment is changed, and the changes in these parameters are rapid once the wavefield enters the elastic sheets. These rapid changes in parameters can be due to amplitude attenuation and decrease in energy. The steepnesses of the waves are shown to decrease inside the elastic sheets, assuring that non-linear effects causing wave breaking should not play an important role at any location since $\epsilon \ll 1$ for all incidents measured experimentally.

6.2 Reflection at sheet edge

From Table 5.11 one can observe that the maximum reflection coefficient of 0.494 is found for $T_p = 0.9$ s and sheet type PEHD_1. For all sheet types the highest coefficients are found for $T_p = 0.9$ s, which can mean that a wavefield with low peak period, hence high frequency, give the most reflection from the elastic sheets. It could be that a higher value of sheet thickness h_i should correspond to a larger reflection coefficient, but from the results of reflection coefficient in this thesis that

does not seem to be the case. Even though the Latex sheet is the thinnest sheet, the calculated reflection coefficients for this sheet does not show remarkable deviations from the calculated coefficients for PEHD sheets. In addition the values from measurements at the location in front of elastic sheets does not vary alot from the reference measurements, which could mean that the effect of reflection from the sheet edge generally is low for all four sheets.

6.3 Skewness and kurtosis

The calculated skewness and kurtosis values from Subsection 5.2.6 shows a few deviating values from a Gaussian sea state, but there is still not an equal development, or trend, for all sheets. One can observe that for the thinnest sheets, hence PEHD_1 and Latex, the values of kurtosis start increasing once the wavefield propagates into the elastic sheets. It seems as kurtosis builds up until mid-sheet, and having a maximum bigger than three before values start decreasing again. Having a kurtosis value higher than the kurtosis for a Gaussian sea state implies that it can be assumed more big waves in the wavefield inside the elastic sheets, than for a normal distribution. This gradually increasing curve of kurtosis has also been discovered in earlier studies for waves propagating from deep to shallow water [22] [11]. It could be that an equal statistical development for waves gradually adapting into the elastic material is found. It seems as the evolution of kurtosis can be believed to be energy dependent, and because of the high attenuation rate for PEHD sheets it could be that it does not show for PEHD_2 and PEHD_3.

Evolution of skewness seem to be increasing for some sheets, and decreasing for others. As mentioned there are no typical trends to observe. Hence it seems as skewness is more negative inside elastic sheets for sheet types PEHD_1 and PEHD_2 than for PEHD_3 and Latex. Why the values of skewness are negative for these two sheets, and thus the distribution of the surface elevation is more skewed towards the left than for a normal distribution we can not explain. For the positive values of skewness the distribution of the surface elevation is more skewed towards the right.

Unfortunately, there has not been found earlier studies on calculated kurtosis and skewness for waves in elastic material. Therefore we are not able to compare these calculated values to anything else than statistical values for a Gaussian sea state. Having skewness $\gamma \neq 0$ and kurtosis $\kappa \neq 3$ states that the wavefield is non-Gaussian as it adapts to the elastic environment.

6.4 Phase speed and group velocity

Calculations (3.3.6) and plots (5.2.4) of phase speed c_p and group velocity c_g shows that both are gradually increasing as waves propagate into elastic sheets. This applies for all sheet types and thicknesses. It also appears as the group velocity c_g is approximately half of the phase speed, hence $c_g \approx \frac{1}{2}c_p$ as for free surface gravity waves. This is also discovered in *Lui & Mollo-Christensen's* article [15]. On the other hand *Sree, Law & Shen* [23] found the phase speed for elastic waves to be less than the phase speed for free surface waves, but also increasing as a function of space. In this thesis the phase speed for elastic waves is found to be bigger than the

free surface phase speed, but agrees with the spatial increase.

Why the increase in phase speed and group velocity one should ask. It might seem more intuitive that both the phase speed and group velocity should decrease as waves propagate into an elastic cover where surface friction occurs. Even in the thickest PEHD sheet the phase speed and group velocity increase through the sheet. A possible explanation for the increase could be the elastic material properties making wave propagation faster. It could also be a result of the decrease in energy, since the amplitudes attenuates and since the wavefields are dominated by longer waves than for a free surface, they travel faster through the sheet. By inserting wavenumber k into equations for c_p (3.56) and c_g (3.58) one can be sure that low wavenumbers, hence long waves, have higher phase speed and group velocity than for larger wavenumbers.

6.5 Amplitude attenuation

Measured amplitudes, calculated to be characteristic amplitudes a_c, for the wavefield show a distinct exponential decay through the sheet. The exponential decay fits the theoretical attenuation curve of *Sutherland et.al.* as the kinematic viscosity β is used as a free variable (see Table 5.4). The attenuation curve fits the measurements as the value for kinematic viscosity is increased as a function of both increasing thickness h_i and decreasing peak period T_p. This could mean that viscosity and dissipation from a boundary layer underneath the elastic sheet becomes even more important as the thickness of the surface cover increases, and as the frequency f_p of the wavefield increases. In addition to viscous effects, a rapid decay in amplitude at the start of the elastic sheet is to be observed for all PEHD sheets. This could be explained from the high E-module since this decay does not follow the theoretical attenuation curve. If properties as elasticity were included in the theoretical function for spatial attenuation rate it might have given a better fit to the measurements on PEHD sheets.

Amplitude attenuation can also be observed in both the one-dimensional frequency spectrum and the two-dimensional, linear scaled wavenumber-frequency spectrum as the energy intensity decreases with decreasing peak period T_p through the elastic sheets. One can also observe that energy intensity decreases as a function of sheet thickness, as some of the plots of the wavenumber-frequency spectrum do not show any intensities for PEHD sheets. This observation is also consistent with both the time series plots and the amplitude decay plots where the amplitudes are approaching to zero.

6.6 Non-linear effects

The intensities of the wavenumber-frequency spectrums with a logarithmic scale can be analysed as we know that the harmonic curves makes up a hierarchy of increasing order of steepness, defined by $k_p a_c = \epsilon$. Normalizing the wave solution

(2.1) by multiplying it with wavenumber k we obtain:

$$k\eta = (ak)\eta_1 + (ak)^2\eta_2 + (ak)^3\eta_3 + \mathcal{O}(ak^4), \tag{6.1}$$

where one can observe that the first harmonic is of order ϵ, the second harmonic is of order ϵ^2 and so on. Studying the logarithmic scaled wavenumber-frequency spectrums from measurements on the elastic sheets, one can recognize energy intensities around the first harmonic (k, ω) being of relative intensity ϵ. Which for the Latex and PEHD_1 sheet are approximately of order 10^{-2}, and for PEHD_2 and PEHD_3 are of order 10^{-3} (see Subsection 5.2.1 for values of ϵ). There is also a possibility that energy around the the second harmonic is visible for the Latex sheet, both for $T_p = 1.1$ s and 1.0 s. The second harmonic relative intensity should be of order $\epsilon^2 \approx 10^{-4}$, which one can observe in Figure 5.36 agrees with the relative intensity along the second harmonic curve.

In the wavenumber-frequency plots of the wavefield for the PEHD sheets the resolution is poor, and it is therefore hard to seperate intensities from blurriness. It can though be discussed if there are energy at some higher harmonics shown for PEHD_2 and PEHD_3, or if these intensities are just a result of attenuation or poor spatial resolution. Since the intensities of the harmonics often are observed having a cloudly distribution, the interpretation of these intensities is not certain. The reason for the second harmonic relative intensity can also be discussed. It could be a possibility that the BFI would increase as a function of distance inside an elastic environment, and that this could be investigated if the elastic sheet used in experiments were longer. The reasons for visible non-linearities in logarithmic scaled spectrums needs to be further investigated, and are therefore not further commented.

For the Latex sheet the zeroth harmonic can clearly be observed as a straight line with an approximate relative intensity of 10^{-4}. This is the same intensity as for the second harmonic, and it might be that this harmonic is of order ϵ^2 as observed in plots. It seems to be the case for the PEHD sheets aswell, even though the zeroth harmonic line is not as visible for this sheet type. The zeroth harmonic intensity has also been discovered for waves on finite depth $kh > 1$, in the article *The non-linear Schrödinger method for water kinematics on finite depth* by *Trulsen et.al.* [30]. It should be noted that the propagation of waves in elastic material has been modelled by the non-linear Schrödinger equation in *Wave propagation in a solid ice pack* [15] as earlier mentioned and simulated in several articles [2], [13], so there could be a possibility that the zeroth harmonic is of the same order as concluded in the article of *Trulsen et.al.*. Still the harmonic expansions for waves in elastic material is yet to be derived, but one can still conclude that non-linear effects can be observed from the results in this thesis.

In addition to the energy intensities concentrated around the harmonics, one can also observe intensities not related to the dispersion relation, being distributed as a cloud around the harmonics. This distribution can be found both for the linear scaled and the logarithmic scaled spectrums.

For the logarithmic scaled spectrum a big amount of intensities being equal to the intensities found around the first harmonic, $\mathcal{O}(\epsilon)$, are also to be found at low wavenumbers k and approximately the peak angular frequency ω_p. This is to be found for all elastic sheets, and could be an imprint of attenuation of short waves

since we know that the wavenumber increases through the sheets. The intensities which are not related to harmonics could also be classified as artifacts from the measurements, as earlier observed in measurements from MARIN's Seakeeping and Manoeuvring Basin by *T.M. Taklo et.al.* [2]. If this is the case the amount of artifacts from experiments done for this thesis is much bigger than found by *T.M. Taklo et.al.*, and it is believed that there must be another explanation. Unfortunately, the explanation of these intensities is still not certain and should be further studied before anything can be concluded.

The energy intensities in the linear scaled spectrums are clearly distributed along the dispersion relation, but still one can recognize the distribution as cloudy over a larger frequency area. This type of energy distribution can be seen for all elastic sheets, but is more clear for PEHD_1. The distribution could be due to non-linear effects since it does not follow the first harmonic, but rather seems as its tangent. This is earlier found for non-linear Schrödinger solutions, and it is believed that the results from linear scaled spectrums can be explained by the non-linear terms from this equation [2].

Chapter 7

Conclusions and further work

7.1 Conclusions

This thesis presents an experimental investigation on wave propagation from open water into water covered by an elastic sheet. A JONSWAP-spectrum with three different peak frequencies, f_p, are used and surface elevation is measured as a function of time and space, both on open water and on elastic sheets. Results show that the characteristics of elastic waves gradually changes, and the wavefield becomes non-Gaussian as $\gamma \neq 0$ and $\kappa \neq 3$. Hence the central limit theorem breaks down, and the wavefield can not be assumed to consist of independent contributions. Phase speed and group velocity are concluded to gradually increase as a function of distance inside elastic sheets. Unlike rates of amplitude attenuation, which show a rapid attenuation due to effects of elasticity at water-sheet boundary. Non-linearities do occur as waves propagate into new surrondings, including into a surface covered by an elastic sheet. Relative energy intensities from zeroth, first and second harmonics are discovered from the surface elevation over the elastic sheets, and are concluded to follow the same order of steepness as derived in the article *The nonlinear Schrödinger method for water wave kinematics on finite depth* of *Trulsen et.al.*. Accordingly the zeroth, first and second harmonic is of $\mathcal{O}(\epsilon^2)$, $\mathcal{O}(\epsilon)$ and $\mathcal{O}(\epsilon^2)$, respectively. In addition, the form of the linear scaled energy distribution in the (k, ω)-domain shows similarity with solutions of the non-linear Schrödinger equation. The similarity being energy distributed as a cloud around the first harmonic. Calculation of Benjamin-Feir Index is done, and small instabilities are found inside elastic sheets. It could be a possibility that the effect of these instabilities can develop if propagation distance inside the elastic environment were longer. Wave characteristics, evolution of phase speed and group velocity show that waves gradually adapts to the new elastic surroundings, as mentioned parameters are a function of distance x into the elastic sheets covering the surface.

7.2 Further work

To follow up this investigation on wave-ice interaction, measurements should be taken with an even higher resolution both for open water measurements in front of elastic sheets and on the elastic sheets. In addition the duration of the surface elevation measurements and the length of the elastic sheets should be extended, to be able to investigate the imprint of non-linear effects found in this thesis. Benjamin-

Feir Index could then be further investigated to unveil if occasions where extreme waves occur are to be found, and hence could be the reason for ice cover breakup. The derivation of harmonics for elastic waves should also be derived to compare results with theoretial values, and to prove the relative intesities of the harmonics from logarithmic scaled spectrums.

Appendix A

Input-file

A.1 JONSWAP

In this particular experiment an irregular and stationary wavefield based on the JONSWAP-spectrum is used to provide propagating waves in the tank. The numerical input, which is uploaded in WaveLab, is made by using Matlab and consists of signals representing voltage V to make irregular waves in the wave tank. When making the signal file in Matlab propagation time, peak period and amplitude can be chosen. This way convergence of different parameters, such as kurtosis and skewness, can be checked for the input-file and the propagation time can be chosen to assure converged results.

A.1.1 Input-file

```
1
2       % JONSWAP-spectrum and time series
3       % Saving the time series in a usable format for the paddle.
4
5       % Formula for the JONSWAP-spectrum from
6       % http://www.codecogs.com/library/engineering/fluid_mechanics/waves
7       % /spectra/jonswap.php
8
9       % Parameters
10      Tp = 1.0; % Peak period
11      T_min = 30; % How many minutes the time series should last
12      N = 3000; % Number of points in spectrum
13      alpha = 0.001; % Amplitude factor
14      V_0 = 5.5; % Voltage in mid-position
15      starttime = 30; % Number of seconds before the series is recorded
16      SampleRate_JONSWAP = 50;
17      delta_t = 1/SampleRate_JONSWAP;
18
19      g = 9.81;
20      gamma = 3.3;
21      beta = 5/4;
22      omega_p = 2*pi/Tp;
23      % Frequencies in the sum
```

```
24      omega_n = linspace(omega_p*0.64,omega_p*2.9,N)';
25      sigma = ones(size(omega_n));
26      sigma(omega_n<=omega_p) = 0.07;
27      sigma(omega_n>omega_p) = 0.09;
28      delta_n = rand(N,1)*2*pi; % Phase shifting vector
29
30      % Calculating spectrum
31      a = exp(-(omega_n-omega_p).^2./(2*omega_p^2*sigma.^2));
32      % The spectrum, which is the weights on the different omega_n
33      S = alpha*g^2*omega_n.^(-5).*exp(-beta*omega_p^4*omega_n.^(-4))...
34          .*gamma.^a;
35
36      % Making time series
37      T = T_min*60; % Length of time series in seconds
38      t = delta_t:delta_t:T+starttime; % time vector in seconds
39      ant_t = length(t); % number of points in the time vector
40      % S_n is a matrix where the coloumns are the values in S
41      [kast S_n] = meshgrid(1:ant_t,S);
42      % DELTA_n is a matrix where the coloumns are the values in delta_n
43      [kast DELTA_n] = meshgrid(1:ant_t,delta_n);
44      tension = V_0 +sum(sqrt(S_n).*cos(omega_n*t+DELTA_n));
45
46      % Ramp up from mid-position at start
47      % number of seconds to ramp up the movement
48      oppramp_tid = 3;
49      opprampefaktor = linspace(0,1,oppramp_tid*SampleRate_JONSWAP);
50      tension(1:length(opprampefaktor)) = ...
51              V_0+(tension(1:length(opprampefaktor))-V_0)...
52              .*opprampefaktor;
53
54      % Ramp down to mid-position in the end
55      % number of seconds to ramp down the movement
56      nedramp_tid = 3;
57      nedrampefaktor = linspace(1,0,nedramp_tid*SampleRate_JONSWAP);
58      tension(end-(length(nedrampefaktor)-1):end) = ...
59              V_0+(tension(end-(length(nedrampefaktor)-1):end)-V_0)...
60              .*nedrampefaktor;
```

Appendix B

Post processing

After the time series of surface elevation is carefully studied the data is processed by interpolating random dropouts that does not seem to fit in to the surface elevation, and are classified as errors from the measurement probes.

B.1 InterpolateDropOuts

```
1     function [eta_out] = InterpolateDropouts(dt,eta,
2     UpperThreshold, LowerThreshold, InnerThreshold)
3
4     % This function removes peaks and dropouts by setting them
5     % to NaN values and interpolating them afterwards.
6
7     % t is the time array for our measured surface elevation
8     % eta is the surface displacement matrix containing 4
9     % coloumns of probes
10    % Uppertheshold: highest peak allowed
11    % Innertheshold: maximum difference allowed between two
12    %neighbouring points
13    T = length(eta)*dt;
14    t = linspace(0,T,length(eta));
15
16    InterpolationMethod = 'pchip';
17    for ProbeNo = [1, 2, 3, 4]
18        for i=1:length(eta)-1
19            if abs(eta(i+1,ProbeNo) - eta(i,ProbeNo)) > InnerThreshold ||..
20                eta(i,ProbeNo) > UpperThreshold || eta(i,ProbeNo) < ...
21                LowerThreshold || abs(eta(i,ProbeNo) -eta(i+1,ProbeNo)) >..
22                InnerThreshold
23
24                eta (i, ProbeNo ) = NaN;
25
26            end
27        end
28
29    eta(any(isnan(eta),2),ProbeNo) = NaN;
30    eta_out(:,ProbeNo) = interp1(t,eta(:,ProbeNo),t,InterpolationMethod);
31
```

```
32          for j = 1:length(eta_out)
33              if (eta_out(j,ProbeNo)) > UpperThreshold || ...
34                  eta_out(j,ProbeNo) < LowerThreshold
35
36                  eta_out(j,ProbeNo) = 0;
37              end
38          end
39      end
40
41      end
```

Bibliography

[1] I.E. Alber. "The effects of randomness on the stability of two dimensional surface wavetrains". In: *A. Mathematical and Physical Sciences* 363 (1978). Proceedings of the Royal Society of London, pp. 525–546.

[2] T.M A.Taklo et al. "On dispersion relation of directional surface gravity waves". In: *J. Fluid Mech. Cambridge University Press* Vol. 812 (2017).

[3] T.B. Brooke and J.E. Feir. "The disintegration of wave trains on deep water 1. Theory". In: *Journal of Fluid Mechanics* 27.3 (1967), pp. 417–430.

[4] G. Broström and K. Christensen. "Waves in sea ice". In: *met.no report, Norwegian Meteorological Institute* No.5 (Mar. 2008).

[5] K. Dysthe, H.E. Krogstad, and P. Müller. "Oceanic rogue waves". In: *Journal of Fluid Mechanics* 40 (2008), pp. 287–310.

[6] K.B. Dysthe et al. "Evolution of a narrow-band spectrum of random surface gravity waves". In: *J. Fluid Mech., Cambridge University Press* Vol. 478 (2003).

[7] B. Gjevik. *Viskøse væsker og elastiske stoffer*. Lecture notes MEK4020. 2002. URL: https://www.uio.no/studier/emner/matnat/math/MEK2200/h07/undervisningsmateriale/mek2200.1.pdf.

[8] J. Grue et al. "Kinematics of extreme waves in deep water". In: *Applied Ocean Research* 25.6 (2003), pp. 355–366.

[9] K. Hasselmann et al. "Measurements of wind-wave growth and swell decay during the Joint North Sea Wave Project (JONSWAP)". In: *Ergänzungsheft 8-12* (1973).

[10] F. Irgens. *Fasthetslære*. Edition 7. Chapter 18 "Spenninger i bjelker". Tapir akademisk forlag, 2007.

[11] S. Jorde. *Kinematikken i bølger over en grunne*. Master's thesis. 2018.

[12] H.E. Krogstad and O.A. Arntsen. "Linear Wave Theory Part B: Random Waves and Wave Statistics". Norwegian University of Science and Technology. 2000.

[13] H.E. Krogstad and K. Trulsen. "Interpretations and observations of ocean wave spectra". In: *Ocean Dynamics* (2010). Springer.

[14] J.D. Logan. *Applied mathematics*. Fourth Edition. John Wiley and Sons, 2013.

[15] A.K Lui and E. Mollo-Christensen. "Wave propagation in a solid ice pack". In: *Journal of physical oceanography* (1988).

[16] N. Mori and P.A.E. M.Janssen. "On Kurtosis and Occurence of Probability of Freak Waves". In: *American Meteorological Society* (2006).

[17] A. Naess and T. Moan. *Stochastic dynamics of marine structures*. Cambridge University Press, 2013.

[18] M.K. Ochi. *Ocean waves: the stochastic approach*. Vol. 6. Cambridge University Press, 2005.

[19] S. Olluri. *Freak waves in bimodal sea*. Master's thesis. 2016.

[20] M. Onorato et al. "Observation of strongly non-Gaussian statistics for random sea surface gravity waves in wave flume experiments". In: *Physical Review E* 70.6 (2004), p. 067302.

[21] G.K. Pedersen. "Hydrodynamic wave theory". Lecture notes MEK4320. URL: https://www.uio.no/studier/emner/matnat/math/MEK4320/h15/undervisningsmateriale/kompendium.pdf.

[22] A. Rausdøl. *Freake bølger over variabelt dyp*. Master's thesis. 2014.

[23] K.K. Sree Dahrma, A. Wing-Keung Law, and H.H. Shen. "An experimental study on gravity waves through a floating viscoelastic cover". In: *Elsevier B.V.* (2018).

[24] S. Støle-Hentschel et al. "Extreme wave statistics of counter-propatating, irregular, long-crested sea states". In: *Physics of Fluids, American Institute of Physics* Vol.30 (2018).

[25] G. Sutherland et al. "The attenuation of monochromatic surface waves due to the presence of an inextensible cover". In: *Wave motion* 68 (2017), pp. 88–96.

[26] T.M. Taklo et al. "Measurements of the dispersion relation for random surface gravity waves". In: *J.Fluid Mech. Cambridge University Press* Vol. 766 (2015).

[27] A. Toffoli et al. "Extreme waves in random crossing seas: Laboratory experiments and numerical simulations". In: *Geophysical Research Letters* 38.6 (2011).

[28] K. Trulsen. "Elementary description of waves". Lecture notes MEK4350. URL: https://www.uio.no/studier/emner/matnat/math/MEK4350/h18/pensumliste/waves.pdf.

[29] K. Trulsen. "Weakly nonlinear and stochastic properties of ocean wave fields. Application to an extreme wave event". In: *Waves in Geophysical Fluids*. Springer, 2006, pp. 49–106.

[30] K. Trulsen, O.T. Gundersen, and M.G. Velarde. "The nonlinear Schrödinger method for water wave kinematics on finite depth". In: *Wavemotion* 33 (2001), pp. 379–395.

[31] P. Wadhams. "How does Arctic sea ice form and decay". In: *Retrieved May* 19.2008 (2003), pp. 275–332.

[32] P. Wadhams, F. Parmiggiani, and G. De Carolis. "The use of SAR to measure ocean wave dispersion in frazil–pancake icefields". In: *Journal of physical oceanography* 32.6 (2002), pp. 1721–1746.

[33] R. Wang and H.H. Shen. "Gravity waves propagating into an ice-covered ocean; a vicoelastic model". In: *J. Geophys. Res.* 115 (2010).

List of Figures

List of Tables